

*Existence, bifurcation, and geometric evolution of quasi-bilayers in the multicomponent functionalized Cahn–Hilliard equation*

**Keith Promislow & Qiliang Wu**

**Journal of Mathematical Biology**

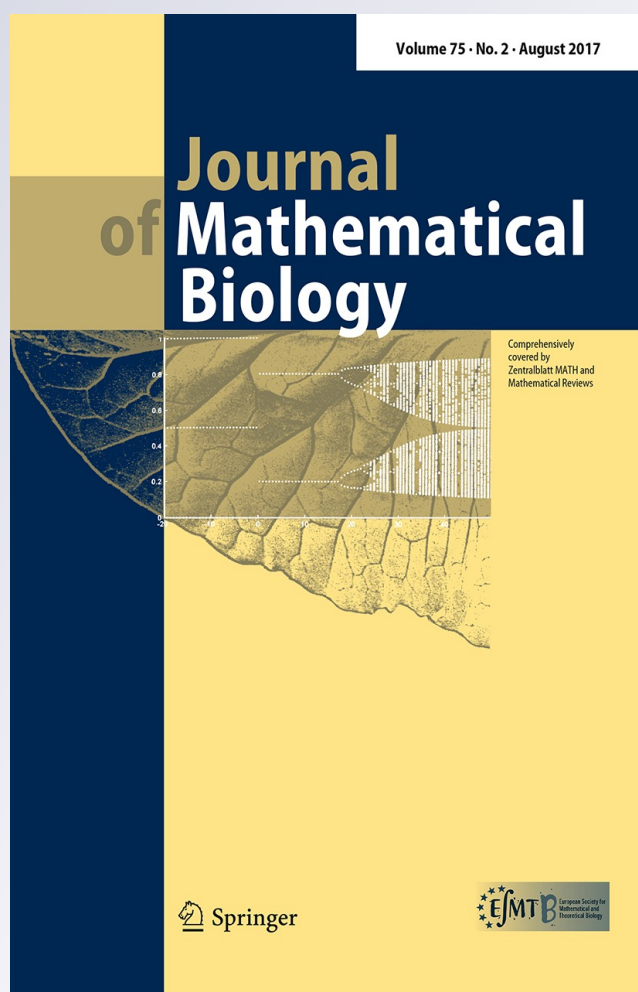
ISSN 0303-6812

Volume 75

Number 2

J. Math. Biol. (2017) 75:443–489


DOI 10.1007/s00285-016-1089-y



**Your article is protected by copyright and all rights are held exclusively by Springer-Verlag Berlin Heidelberg. This e-offprint is for personal use only and shall not be self-archived in electronic repositories. If you wish to self-archive your article, please use the accepted manuscript version for posting on your own website. You may further deposit the accepted manuscript version in any repository, provided it is only made publicly available 12 months after official publication or later and provided acknowledgement is given to the original source of publication and a link is inserted to the published article on Springer's website. The link must be accompanied by the following text: "The final publication is available at [link.springer.com](http://link.springer.com)".**



# Existence, bifurcation, and geometric evolution of quasi-bilayers in the multicomponent functionalized Cahn–Hilliard equation

Keith Promislow<sup>1</sup> · Qiliang Wu<sup>1</sup> 

Received: 21 December 2015 / Revised: 20 August 2016 / Published online: 31 December 2016  
© Springer-Verlag Berlin Heidelberg 2016

**Abstract** Multicomponent bilayer structures arise as the ubiquitous plasma membrane in cellular biology and as blends of amphiphilic copolymers used in electrolyte membranes, drug delivery, and emulsion stabilization within the context of synthetic chemistry. We present the multicomponent functionalized Cahn–Hilliard (mFCH) free energy as a model which allows competition between bilayers with distinct composition and between bilayers and higher codimensional structures, such as co-dimension two filaments and co-dimension three micelles. We construct symmetric and asymmetric homoclinic bilayer profiles via a billiard limit potential and show that co-dimensional bifurcation is driven by the experimentally observed layer-by-layer pearling mechanism. We investigate the stability and slow geometric evolution of multicomponent bilayer interfaces within the context of an  $H^{-1}$  gradient flow of the mFCH, addressing the impact of aspect ratio of the amphiphile (lipid or copolymer unit) on the intrinsic curvature and the codimensional bifurcation. In particular we derive a Canham–Helfrich sharp interface energy whose intrinsic curvature arises through a Melnikov parameter associated to amphiphile aspect ratio.

**Keywords** Functionalized Cahn–Hilliard energy · Canham–Helfrich energy · Multi-component bilayer · Billiard limit

**Mathematics Subject Classification** 92B05 · 35B36 · 35B40 · 53A05

---

✉ Qiliang Wu  
qwu@math.msu.edu

<sup>1</sup> Department of Mathematics, Michigan State University, 619 Red Cedar Road, East Lansing, MI 48824, USA

## 1 Introduction

Amphiphilic molecules, such as lipids and functionalized polymers, are central to the self-assembly of intricately structured, solvent accessible nano-scaled morphologies and network structures. Indeed, Nafion, the generic ion separator in PEM fuel cells is comprised of a hydrophobic fluorocarbon polymer-backbone functionalized by  $SO_3H$  acidic side-chains. The result is a plastic-like ionomer that imbibes water to achieve solvent-accessible surface areas on the order of  $1000\text{ m}^2/\text{gram}$ , the highest for any manufactured material (Knox and Voth 2010). By combining hydrophilic and hydrophobic groups, this amphiphilic molecules, which we will refer to as amphiphiles, serve as surfactants, lowering interfacial energy, often to negative values (Zhu and Hayward 2008) and self-assembling into a wide range of network morphologies that balance packing entropy against hydrophilicity. The resulting materials have received extensive attention, for their wide applications to pharmaceuticals, emulsion stabilization, detergent production and energy conversion devices (Alexandridis and Lindman 2000; Ameduri 2009; Peet et al. 2009; Rubatat et al. 2004; Promislow and Wetton 2009; Jain and Bates 2004; Laschewsky 2003; Li et al. 2004; Lutz and Laschewsky 2005). Of course amphiphiles play a central role in cellular biology, particularly in plasma membranes. These complex multicomponent systems are highly heterogeneous in the lipid distribution and composition, yielding clustering of particular lipids that is associated to intrinsic curvature of the membrane (Hanton et al. 2005; Leventis and Grinstein 2010; Koldsø et al. 2014). Moreover, the interplay between species of lipids is also critical to the structure of the endoplasmic reticulum (Maneta-Peyret et al. 2014) membrane signaling and trafficking (Simons and Vaz 2004) and has been proposed as a possible pathways to cell division in primitive single-celled organisms (Budín and Szostak 2011) while cholesterol regulates influenza A fusion in late endosomes by inducing negative spontaneous curvature (van Meer et al. 2008).

### 1.1 Multicomponent functionalized Cahn–Hilliard free energy

Many phase-field based models of cell membranes are based upon a “single-layer” formulation (Wang and Du 2008; Lowengrub et al. 2009; Ryham et al. 2012), in which a co-dimension one interface separates two solvent phases, with the inside and the outside of the cell identified with a distinct phase field label. However many of the fundamental properties of membranes arise from their bilayer nature, in which an amphiphilic phase forms a two-sheeted co-dimension one interface that interpenetrates and separates a single solvent phase. Bilayer models of membranes have several advantages over single-layer models including a strong binding energy between the constituent layers which affords a natural mechanism to modulate the bilayer width, the possibility to perforate the membrane, or to reorganize into a higher co-dimensional structure such as a filament or a micelle, see Fig. 1.

We propose the multicomponent functionalized Cahn–Hilliard (mFCH) free energy as a model for the energy landscape of multicomponent blends of amphiphiles (particularly lipids). The mFCH free energy encompasses competition not only among morphologies with distinct co-dimensions but also couples the rearrangement of

amphiphiles on the surface of network structure to the stability and geometric evolution of the underlying surface. This work focuses on co-dimension one interfaces, and addresses the competition with higher co-dimensional morphologies through the *pearling* bifurcations that lead to filamentation or budding into micelles. The mFCH model is partially phenomenological, but incorporates the key elements of packing entropy and hydrophilicity in a transparent and mathematically elegant manner. Indeed, lipids have typically been classified based upon their aspect ratios (Mouritsen 2011), with bilayers associated with an aspect ratio near one, and smaller values of the aspect ratio associated with morphological bifurcations into filaments and micelles. However lipid aspect ratio also leads to non-zero intrinsic curvature of bilayers when the two sheets of the bilayer are formed of distinct mixtures. While the issues of intrinsic curvature and co-dimension bifurcation are both impacted by lipid aspect ratio, they have typically been studied independently, see Mouritsen (2011) and Koldsø et al. (2014) for example. It is fundamental that a model distinguish between conditions under which an increase in aspect ratio of a lipid component would induce intrinsic curvature and when it would lead the bilayer to bifurcate into a higher co-dimensional structure, such as a filament or a micelle. The mFCH supports each of these distinct phases in a compact continuum formulation.

The scalar functionalized Cahn–Hilliard (FCH) free energy is a well-studied model for mixtures of a single amphiphilic phase with a solvent (Promislow and Wetton 2009; Gavish et al. 2011; Dai and Promislow 2013; Promislow and Yang 2014; Doelman et al. 2014; Promislow and Wu 2015). The FCH corresponds to a special case of the model proposed by Teubner and Strey (1987) and later Gompper and Schick (1990); motivated by small-angle X-ray scattering (SAXS) data of micro-emulsions of soapy-oil within water, they suggested a free energy for the soapy-oil volume fraction  $u \in H^2(\Omega)$  in the form

$$\mathcal{F}_{GS}(u) = \int_{\Omega} \varepsilon^4 \frac{1}{2} |\Delta u|^2 + \varepsilon^2 G_1(u) \Delta u + G_2(u) \, dx, \tag{1.1}$$

where the function  $G_1$  takes distinct values in the soapy-oil phase  $u \approx 1$  and the water phase  $u = 0$ . The parameter  $\varepsilon > 0$  scales homogeneously with space, and denotes the ratio of the interfacial thickness to the size of the domain  $\Omega \subset \mathbb{R}^d$ , generically  $\varepsilon \ll 1$ . This free energy includes a vast parameter space, and the functionalized Cahn–Hilliard corresponds to a simplifying choice  $G_1 = -W'(u)$ , for  $W$  a double-well potential with unequal depth wells at  $u = 0$  and  $u = b > 0$  and  $G_2 = \frac{1}{2}(W'(u))^2 - \varepsilon^p P(u)$ . This form corresponds to a perturbation of a perfect square. Indeed, slightly redefining  $W$  and  $P$ , see Promislow and Wu (2015) for details, this special case of the Gompper and Schick free energy can be written as the FCH free energy

$$\mathcal{F}(u) = \int_{\Omega} \frac{1}{2} \left( \varepsilon^2 \Delta u - W'(u) \right)^2 - \varepsilon^p \left( \frac{1}{2} \varepsilon^2 \eta_1 |\nabla u|^2 + P(u) \right) \, dx. \tag{1.2}$$

The FCH admits a wide range of potential minimizers corresponding to bilayers, filaments, micelles and their local defects which, to leading order, renders the dominant quadratic term zero; that is, they solve

$$\varepsilon^2 \Delta u - W'(u) = O(\varepsilon), \tag{1.3}$$

where the double-well  $W$  is the mixing potential, encoding the dominant components of the packing energy of the lipid-solvent mixture corresponding to the lipid volume fraction  $u$ . These solutions are asymptotically close to the critical points of the corresponding Cahn–Hilliard type energy

$$\mathcal{E}(u) = \int_{\Omega} \frac{\varepsilon^2}{2} |\nabla u|^2 + W(u) \, dx, \tag{1.4}$$

and correspond to optimal packings of lipid structures. The functionalization terms are perturbations of the dominant quadratic, with the values  $p = 1$  and  $p = 2$  corresponding to the strong and weak functionalizations respectively. In the strong functionalization these terms dominate the  $O(\varepsilon^2)$  Willmore residual in the quadratic term, while for the weak functionalization the terms asymptotically balance. In both cases the functional terms encode perturbative energy preferences among the optimal structures defined in (1.3). For  $\eta_1 > 0$  the first functionalization term rewards variation in  $u$  associated with the generation of co-dimension one interface or higher codimension hyper-surfaces. This term encodes the strength of the hydrophilic-solvent interaction. The second functionalization term, given by the potential  $P$ , is typically taken in the simplified form  $P = \eta_2 W$ , incorporates energetic deviations among the solutions of (1.3), assigning lower energies to morphologies residing in regions where  $P > 0$ .

The scalar FCH free energy supports quasi-minimizing bilayer solutions that correspond to finite-width versions of the co-dimension-one sharp interface,  $\Gamma$  immersed in  $\Omega \subset R^d$ . In the  $\varepsilon \rightarrow 0$  limit, the FCH evaluated at these bilayer solutions tends to a Canham–Helfrich type limit (Canham 1970),

$$\mathcal{E}_{\text{Helfrich}}(\Gamma) := \int_{\Gamma} c_0(H(s) - c_1)^2 + c_2 + c_3 K(s) \, dS \tag{1.5}$$

where  $H$  and  $K$  are the mean and Gaussian curvatures of  $\Gamma$ , with  $c_0, c_1, c_2$ , and  $c_3$  denoting constants; in particular  $c_1$  is the intrinsic curvature, the value of the mean curvature that corresponds to zero bending energy, see Gavish et al. (2011) and Fig. 1. However for the scalar FCH, the bilayer must be symmetric about its midplane and the intrinsic curvature,  $c_1$ , is zero in the sharp interface limit. Non-zero intrinsic curvature requires symmetry breaking, and a bilayer that is asymmetric about its midplane must be composed of more than one type of amphiphilic species.

An investigation of the interaction between intrinsic curvature in bilayers and morphological bifurcation, requires a multi-component extension of the FCH free energy that encompasses a single solvent phase with  $N$  lipid species. Similar to the scalar case, we introduce a vector-valued phase function  $\mathbf{u} \in [H^2(\Omega)]^N$  with the  $i$ 'th component denoting the local volume fraction of lipid type  $i = 1, \dots, N$ , and the associated multi-component weak FCH free energy

$$\mathcal{F}_M(\mathbf{u}) = \int_{\Omega} \frac{1}{2} |\varepsilon^2 \Delta \mathbf{u} - \nabla_{\mathbf{u}} W(\mathbf{u}) + \varepsilon \mathbf{V}(\mathbf{u})|^2 - \varepsilon^2 \left( \varepsilon^2 \frac{\eta_1}{2} |\nabla \mathbf{u}|^2 + \eta_2 W(\mathbf{u}) \right) \, dx. \tag{1.6}$$

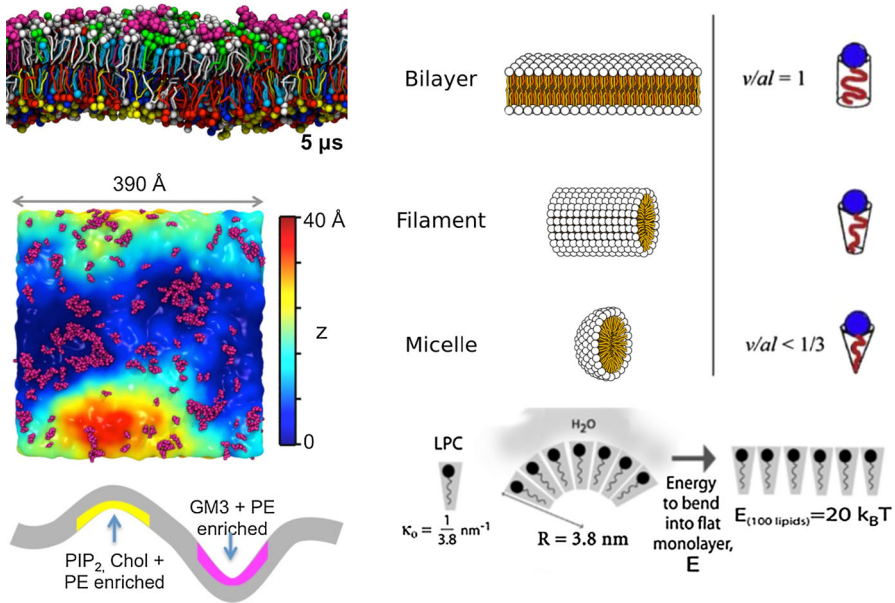


**Fig. 1** (Left-panel) The initial and final structures of a plasma membrane from simulations (Koldsø et al. 2014), composed of six types of lipids: POPC (light gray), POPE (red), POPS (blue), GM3 (magenta), Sph (green), PIP<sub>2</sub> (yellow), and Cholesterol (cyan). The inner leaflet has initial composition POPC:POPE:Sph:GM3:Chol in ratios (40:10:15:10:25) while the outer leaflet had initial composition POPC:POPE:POPS:PIP<sub>2</sub>:Chol in ratios (10:40:15:10:25). The system was relaxed for 5 μs, and the top image shows a snap-shot of the through-plane structure of the two leaflets, the middle image is a top down view color-coded according to the deformation of the membrane along the normal direction, with GM3 lipids depicted in magenta and other lipids not shown. The bottom image relates the correlation between lipid type and membrane curvature. Reprinted from Koldsø et al. (2014). PLoS Computational Biology is an open access journal. (Right-panel-top) Mouritsen’s characterization of morphologies generated by lipid-solvent mixtures based upon the aspect ratio,  $V/al$ , of the truncated cone of volume  $V$ , cap area  $a$ , and length  $l$ , that best contains the hydrophobic (tail) component (Mouritsen 2011). In the mFCH free energy, (6.3), the aspect ratio is incorporated into both the intrinsic curvature, via the non-solenoidal perturbation  $\mathbf{V}$ , and the selection of co-dimension through pearling bifurcations mediated via the average value of  $P(\mathbf{u})$  over the profile, with co-dimension 3 micelles correspond to small values of  $P$ , and increasing values leading to co-dimension 2 filaments, and co-dimension 1 bilayers. The left half of the panel consists of three public domain figures created by Mariana Ruiz Villarreal and the right half is reprinted from Mouritsen (2011) with permission from John Wiley and Sons. (Right-bottom) For LPC (Cohen and Melikyan 2004), the relation between the aspect ratio of the hydrophobic cone, the intrinsic curvature, and the energy required to flatten the layer. Reprinted from Cohen and Melikyan (2004) with permission from Springer (colour figure online)

For the derivation of the mFCH free energy from the multi-component Gommper-Schick (mGS) free energy, see “Appendix”. An essential distinction between the FCH and mFCH is that, vector-valued functions need not to be the gradient of a scalar potential; consequently we consider the mFCH with a bulk potential of the form  $\nabla_{\mathbf{u}} W(\mathbf{u}) - \varepsilon \mathbf{V}$ , where the vector field  $\mathbf{V}$  is non-solenoidal, that is  $\nabla \times \mathbf{V} \neq 0$ , and hence is not the gradient of a scalar potential.

The associated  $H^{-1}$  gradient flow of the weak mFCH free energy is the system

$$\mathbf{u}_t = \Delta \frac{\delta \mathcal{F}_M}{\delta \mathbf{u}}, \tag{1.7}$$

subject to periodic boundary conditions on  $\Omega \subset \mathbb{R}^d$ , where the variational derivative takes the form

$$\begin{aligned} \frac{\delta \mathcal{F}_M}{\delta \mathbf{u}} &= \left( \varepsilon^2 \Delta - \nabla_{\mathbf{u}}^2 W(\mathbf{u}) + \varepsilon (\nabla_{\mathbf{u}} \mathbf{V}(\mathbf{u}))^T \right) \left( \varepsilon^2 \Delta \mathbf{u} - \nabla_{\mathbf{u}} W(\mathbf{u}) + \varepsilon \mathbf{V}(\mathbf{u}) \right) \\ &\quad + \varepsilon^2 \left( \varepsilon^2 \eta_1 \Delta \mathbf{u} - \eta_2 \nabla_{\mathbf{u}} W(\mathbf{u}) \right). \end{aligned} \tag{1.8}$$

The flow is local in space and conserves the  $\varepsilon$ -scaled total mass-vector

$$\mathcal{M}(\mathbf{u}) := \frac{1}{\varepsilon} \int_{\Omega} \mathbf{u} dx, \tag{1.9}$$

of the  $N$  amphiphilic species. Sections 2 and 4 address the case of  $N \in \mathbb{N}^+$  while Sect. 3 focuses on the case  $N = 2$  for notational simplicity.

### 1.2 Quasi-bilayers

Our analysis addresses the construction, linear stability, and slow evolution of families of *quasi-minimizers*: distributions  $\mathbf{u} \in [H^2(\Omega)]^N$  with sufficiently small free energy and low lipid mass fraction,  $\mathcal{M}$  see (1.9). More specifically, given a fixed constant  $C > 0$ , the associated set of quasi-minimizers is given as

$$\mathcal{Q}_C := \left\{ \mathbf{u} \in [H^2(\Omega)]^N \mid |\mathcal{M}(\mathbf{u})| \leq C \text{ and } \mathcal{F}_M(\mathbf{u}) \leq C\varepsilon^3 \right\}. \tag{1.10}$$

The energy  $\mathcal{F}_M$  is bounded from below for fixed values of  $\varepsilon > 0$ , but can be negative, see Promislow and Zhang (2013) for a discussion of lower bounds for the scalar FCH.

Candidates for quasi-minimizers are readily constructed from approximate solutions of the stationary weak mFCH equation,

$$\frac{\delta \mathcal{F}_M}{\delta \mathbf{u}} = \varepsilon^2 \mathbf{m}, \tag{1.11}$$

where  $\mathbf{m} \in \mathbb{R}^N$  can be viewed as an  $\varepsilon^2$ -scaled Lagrange multiplier associated to the mass constraint imposed by the mFCH gradient flow. We focus our attention on a class of quasi-minimizers called *quasi-bilayers*. These are constructed by fixing an admissible co-dimension one base interface  $\Gamma$  immersed in  $\Omega$ , changing to local coordinates  $(z, s)$ , where  $z$  is  $\varepsilon$  scaled distance to  $\Gamma$  and  $\mathbf{r}(s) : S \mapsto \Gamma$  is a parameterization of  $\Gamma$ , see Definition 2.1 for details. Within the local variables the Laplacian takes the



form (2.1), and the stationary Eq. (1.11) reduces at lowest order to the second order dynamical system

$$\partial_z^2 \phi_h - \nabla_{\mathbf{u}} W(\phi_h) = 0, \tag{1.12}$$

subject to the condition that  $\phi_h$  is homoclinic to zero. For special cases, the homoclinic solution can be corrected to yield a higher-order approximation to (1.11), however the solenoidal perturbation,  $\varepsilon V$  is not such a case, and persistence of homoclinic solutions under the solenoidal perturbation requires the introduction of a Melnikov parameter. To account for the necessary degrees of freedom within the system, we introduce the perturbed homoclinic  $\Phi_h = \Phi_h(z, \varepsilon; \mathbf{m})$ , of the solenoidal ODE,

$$\partial_z^2 \Phi_h + \varepsilon a \partial_z \Phi_h - \nabla_{\mathbf{u}} W(\Phi_h) + \varepsilon \mathbf{V}(\Phi_h) = -\varepsilon^2 \left[ \nabla_{\mathbf{u}}^2 W(0) \right]^{-1} \mathbf{m}, \tag{1.13}$$

where the mass constraint  $\mathbf{m}$  is viewed as a parameter that prescribes the far-field behavior

$$\Phi_{\infty}(\varepsilon; \mathbf{m}) := \lim_{z \rightarrow \infty} \Phi_h(z, \varepsilon; \mathbf{m}) = \varepsilon^2 [\nabla_{\mathbf{u}}^2 W(0)]^{-2} \mathbf{m} + O(\varepsilon^3). \tag{1.14}$$

Conversely the Melnikov parameter  $a$  is fixed by the choice of the homoclinic profile  $\phi_h$  and more significantly by  $V$  through the expansion

$$a = a_0 + \mathcal{O}(\varepsilon), \quad a_0 := -M_1^{-1} \int_{\mathbb{R}} \mathbf{V}(\phi_h(z)) \cdot \partial_z \phi_h(z) dz, \quad M_1 := \int_{\mathbb{R}} |\partial_z \phi_h(z)|^2 dz. \tag{1.15}$$

The *quasi-bilayer* profiles are the vector-valued smooth functions  $\mathbf{u}_q \in [H^2(\Omega)]^N$  obtained by the “dressing” of an admissible interface  $\Gamma$ , defined in Definition 2.1, with the profile  $\Phi_h(z, \varepsilon; \mathbf{m})$  via the relations

$$\begin{aligned} & \mathbf{u}_q(x; \varepsilon, \mathbf{m}, \Gamma) \\ &= \begin{cases} \Phi_h(z(x), \varepsilon; \mathbf{m}), & x \in \Gamma_{l_0}, \\ (1 - \chi(\frac{\varepsilon|z(x)|}{l_0}))\Phi_{\infty}(\varepsilon, \mathbf{m}) + \chi(\frac{\varepsilon|z(x)|}{l_0})\Phi_{h,\delta}(z(x), \varepsilon; \mathbf{m}), & x \in \Gamma_{3l_0} \setminus \Gamma_{l_0}, \\ \Phi_{\infty}(\varepsilon; \mathbf{m}), & x \in \Omega \setminus \Gamma_{3l_0}, \end{cases} \end{aligned} \tag{1.16}$$

where the inner region  $\Gamma_{l_0}$  is given in Definition 2.1, and  $\chi : \mathbb{R} \rightarrow \mathbb{R}$  is a smooth cut-off function satisfying  $\chi(r) = 1$  for  $|r| \leq 1$  and  $\chi(r) = 0$  for  $|r| \geq 3$ . The quasi-bilayer profiles are parameterized by  $\{\mathbf{m}, \Gamma\}$ , where  $\mathbf{m}$  controls the far-field value and  $\Gamma$  is an admissible co-dimension one immersion within  $\Omega$  that specifies the bilayer center-line. For fixed  $C, l_0 > 0$  we study the set of quasi-bilayers  $\mathcal{M}_{C,l_0}(\varepsilon)$  defined as

$$\begin{aligned} \mathcal{M}_{C,l_0}(\varepsilon) &:= \{ \mathbf{u}_q(\cdot; \varepsilon, \mathbf{m}, \Gamma) \in C^{\infty}(\Omega) \mid |\mathbf{m}| \\ &\leq C, \Gamma \text{ is an admissible interface with reach } l_0 \}. \end{aligned} \tag{1.17}$$

### 1.3 Main results

In Sect. 2, we establish the persistence of homoclinic solutions under the solenoidal perturbations and verify that each quasi-bilayer is a quasi-minimizer; that is,

$$\mathcal{M}_{C,l_0}(\varepsilon) \subset \mathcal{Q}_C,$$

and moreover their free energy  $\mathcal{F}_M(\mathbf{u}_q)$  admits a Canham–Helfrich sharp interface free energy at leading order. More specifically, introducing the notation

$$\mathbf{M} := \int_{\mathbb{R}} \phi_h(z) dz, \quad \mathbf{B} := [\nabla_{\mathbf{u}}^2 W(0)]^{-2} \mathbf{m}, \quad \phi_{h,1} := \partial_{\varepsilon} \Phi_h|_{\varepsilon=0}, \quad (1.18)$$

which denote, respectively the mass per unit length of the bilayer  $\phi_h$ , the leading-order constant far-field value of  $\Phi_h$ , and the  $O(\varepsilon)$ -order term in the expansion of  $\Phi_h$ , we establish the following Theorem.

**Theorem 1** *Subject to Assumption 2.2, the ODE (1.12) admits the first-order form*

$$\begin{pmatrix} \mathbf{u} \\ \mathbf{v} \end{pmatrix}_z = \begin{pmatrix} \mathbf{v} \\ \nabla_{\mathbf{u}} W(\mathbf{u}) \end{pmatrix}, \quad (1.19)$$

for which the origin is a hyperbolic equilibrium whose stable and unstable manifolds intersect transversely at  $(\phi_h, \phi'_h)$ . For any  $C, l_0 > 0$  there exists  $\varepsilon_0, C_1 > 0$  such that for all  $\varepsilon \in (0, \varepsilon_0)$  the family of quasi-bilayers  $\mathcal{M}_{C,l_0}$  is contained within the set of quasi-minimizers  $\mathcal{Q}_{C_1}$  and the mFCH evaluated at  $\mathbf{u}_q(\mathbf{m}, \Gamma) \in \mathcal{M}_{C,l_0}$  reduces to a Canham–Helfrich sharp interface energy on  $\Gamma$  of the form

$$\mathcal{F}_M(\mathbf{u}_q) = \varepsilon^3 \frac{M_1}{2} \int_S \left[ (H_0(s) - a_0)^2 - (\eta_1 + \eta_2) \right] dS + \mathcal{O}(\varepsilon^4), \quad (1.20)$$

where  $H_0$  is the mean curvature of  $\Gamma$  and the intrinsic curvature  $a_0$  and constant  $M_1$  are defined in (1.15). Moreover the total  $\varepsilon$ -scaled mass takes the form

$$\mathcal{M}(\mathbf{u}_q) = |\Gamma| \mathbf{M} + \varepsilon \left[ |\Omega| \mathbf{B} + |\Gamma| \int_{\mathbb{R}} \phi_{h,1}(z) dz + \int_S H_0(s) dS \int_{\mathbb{R}} z \phi_h(z) dz \right] + \mathcal{O}(\varepsilon^2), \quad (1.21)$$

where  $\mathbf{M}, \mathbf{B}$  and  $\phi_{h,1}$  are defined in (1.18).

Section 3 is restricted to the case  $N = 2$  and focuses on a class of regularized Birkhoff billiard potentials for the mixing wells for which it is possible to construct and explicitly characterize a large family of homoclinic solutions of the corresponding Hamiltonian ODE (1.12). We denote the regularized Birkhoff-billiard potentials as  $\{B_{\delta}(\mathbf{u})\}$ , where  $\delta > 0$  is a smoothing parameter. The Birkhoff billiard potential  $B(\mathbf{u})$  is piece-wise smooth, with a strict local minima at the origin and transitions to a positive constant in a large region, and jumps discontinuously to a fixed negative value across a ‘collision-curve’, see the bottom row of images of Fig. 2. The Hamiltonian structure of

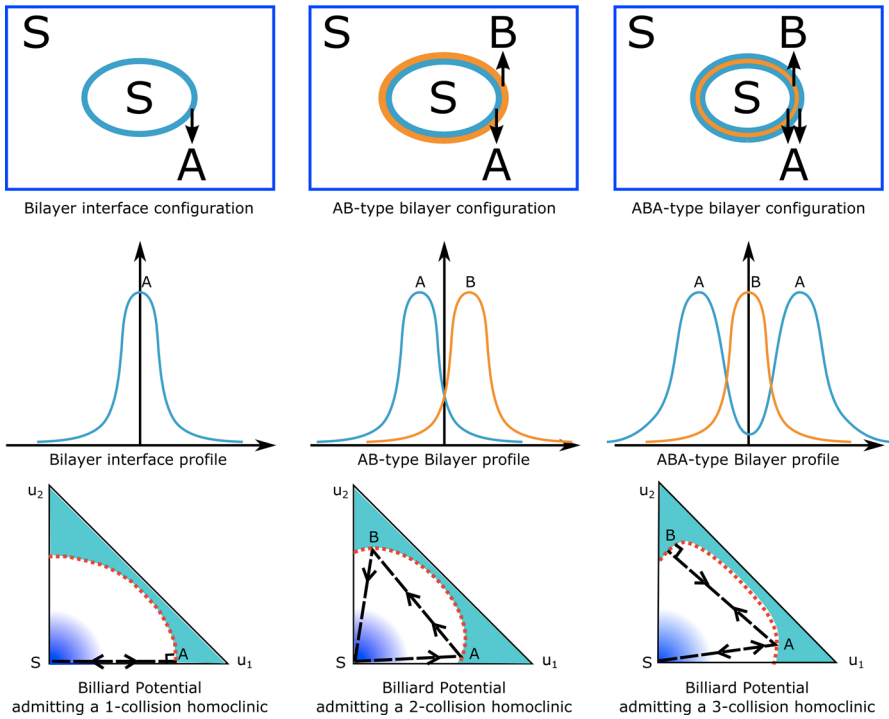


**Fig. 2** The top row depicts the physical domain  $\Omega \subset \mathbb{R}^3$  with a bilayer (left), an AB-type bilayer (middle), and an ABA-type bilayer (right). The solvent phase is denoted by S and A and B denote species of amphiphiles. The middle row depicts the density profile of the solute or solutes (phase A and B) along the scaled normal direction,  $z$ , of the interface given by solutions of (6.5). The bottom row depicts the mixing potential  $W$  as a function of  $\mathbf{u}$ , with the superimposed dashed lines depicting the homoclinic orbits,  $\phi_h$ . The potentials are Birkhoff-billiard potentials, see Definition 3.1 and Fig. 5 in Sect. 3 for more details

(6.5) precludes the orbits homoclinic to the origin from entering the negative- $W$  region and thus they impact the discontinuity in a billiard-like collision. To each collision we associate a “striation” within the corresponding co-dimension one interface, see Fig. 2. Striations have been observed experimentally in blends of polymer blends of  $A - B$  diblock with a  $B - C$  diblock (Zhu and Hayward 2008), with  $A$  representing the most hydrophilic component and  $C$  the most hydrophobic. These multicomponent, di-block blends phase-separate into distinct striated structures which exhibit striation localized pearling bifurcations, as depicted in the left panel of Fig. 3.

Within the context of a regularized-billiard potential  $B_\delta(\mathbf{u})$ , we show the existence of  $n$ -striation bilayers which are homoclinic to the origin, and characterize the spectrum of the associated second variational derivative of  $\mathcal{F}_M$ . We emphasize that the term bilayer refers to the dressing of a co-dimension one admissible interface with a solution  $\Phi_h$  of (1.13) that is asymptotically homoclinic to the origin. The  $n$  in the  $n$ -striation refers to the number of distinct shifts in composition of the bilayer in the through-plane direction. In particular the term striation is only meaningful when the mixing potential  $W$  is a  $\delta \ll 1$  regularized Birkhoff billiard potential. For a given regularized

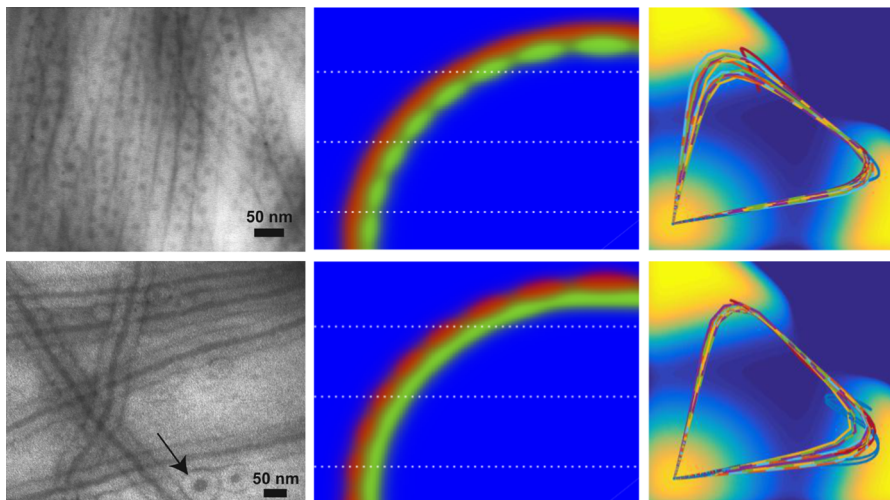


**Fig. 3** (Left) Distinct  $AB$ -type bi-layer filaments, formed from blends of  $PS_{9.5K} - PEO_{5K}$  with  $PS_{56K} - P2VP_{21K}$ , exhibit a layer-by-layer pearling bifurcation into pearled P2VP cores. Reprinted with permission from [Zhu and Hayward \(2008\)](#). Copyright 2008 American Chemical Society. (Center, Right) Numerical simulations of the layer-by-layer pearling of an  $AB$ -type bilayer structure. More specifically, given  $N = d = 2$ ,  $\Omega = [0, 2\pi] \times [0, 2\pi]$ ,  $\varepsilon = 0.2$ ,  $\eta_1 = \eta_2 = 1$ ,  $V(\mathbf{u}) = (-u_2, u_1)^T$  and the mixing well as a regularized-billiard potential with  $\delta = 0.2$ , the simulation of the weak mFCH gradient flow with the initial data that is slightly above, equal to, and slightly below, the target value. The left panels show the physical configurations of the pearled morphologies, where *blue*, *red* and *green* represent respectively the solvent, amphiphile A and amphiphile B. In the right panels, the *horizontal* and *vertical* axis denote  $u_1$  and  $u_2$ , the volume fractions of amphiphile A and B, respectively; the background is the contour plot of  $-W(\mathbf{u})$  with high values in *yellow* and low values in *blue*; the triangular traces depict the orbit of  $\mathbf{u}$  parametrized by  $x_1$  for chosen fixed  $x_2$  along the white *dotted* lines in center panels. The code used in the numerical simulation is developed by Brian Wetton (colour figure online)

Birkhoff-billiard potential, the second variational derivative of the mFCH free energy (1.6) about an  $n$ -striation bilayer  $\psi_{h,\delta}$  yields an operator  $\mathbb{L}$  of the form

$$\mathbb{L} := \frac{\delta^2 \mathcal{F}_M}{\delta \mathbf{u}^2}(\psi_{h,\delta}) = (\mathcal{L}_\delta + \varepsilon^2 \Delta_s)^2 + \mathcal{O}(\varepsilon), \tag{1.22}$$

where  $\Delta_s$  is the Laplace–Beltrami operator associated to  $\Gamma$  and the structural operator associated to  $\psi_{h,\delta}$

$$\mathcal{L}_\delta := \partial_z^2 - \nabla_{\mathbf{u}}^2 B_\delta(\psi_{h,\delta}), \tag{1.23}$$

maps  $[H^2(\mathbb{R})]^2$  to  $[L^2(\mathbb{R})]^2$ . As for the scalar FCH in the weak settings ([Hayrapetyan and Promislow 2014](#)), the negative spectrum of  $\mathbb{L}$  can only arise when the dominant quadratic term is close to zero. Since the Laplace–Beltrami operator is non-positive, negative spectrum occurs only for tensor product eigenfunctions with the leading order form

$$\Psi_{j,k}(z, s) := \psi_j(z)\Theta_k(s) + \mathcal{O}(\varepsilon), \tag{1.24}$$

where  $\psi_j$  is an eigenfunction of  $\mathcal{L}_\delta$  associated to eigenvalue  $\lambda_j \geq 0$  and  $\theta_k$  is a Laplace–Beltrami eigenfunction with eigenvalue  $\beta_k < 0$  for which  $\lambda_j + \varepsilon^2 \beta_k = \mathcal{O}(\sqrt{\varepsilon})$ .

Rigorous statements about the pearling spectrum for the second variation,  $\mathbb{L}$ , for the scalar FCH free energy can be found in [Hayrapetyan and Promislow \(2014\)](#).

These tensor-product eigenmodes of  $\mathbb{L}$  are the pearling eigenvalues, as their high-frequency in-plane oscillation generates a pearled morphology, see [Fig. 3](#) for experimental observations and [\(Promislow and Wu 2015\)](#) for a rigorous construction of pearled morphologies for the scalar FCH. For  $\delta$  sufficiently small we show that  $\mathcal{L}_\delta$  associated to an  $n$ -collision homoclinic possesses precisely  $n$  large positive eigenvalues of order  $\mathcal{O}(\delta^{-2})$  which may be enumerated so that for  $j = 1, \dots, n$ , the corresponding  $j$ 'th eigenfunction  $\{\psi_j\}_{j=1}^n$  is generically localized on the  $j$ -th striation, as corresponds to the experimentally observed striation-localized pearling. More precisely, we establish the following theorem.

**Theorem 2** *Given a Birkhoff-billiard potential  $B(\mathbf{u})$  in the form [Definition 3.1](#) for which the leading-order ODE [\(1.12\)](#) admits a transversal  $n$ -collision homoclinic  $\psi_h$ ; see [Assumptions 3.3](#) and [3.5](#). For sufficiently small  $\delta > 0$ , the leading-order ODE [\(1.12\)](#) with the regularized Birkhoff-billiard potential  $B_\delta(\mathbf{u})$  given in [Definition 3.7](#) admits a unique homoclinic continuation,  $\psi_{h,\delta}$ . The associated linearized operator  $\mathcal{L}_\delta$  defined in [\(1.23\)](#) has real spectrum  $\sigma(\mathcal{L}_\delta) \subset \mathbb{R}$ , and admits precisely  $n$  "collision" eigenvalues,  $\{\lambda_1(\delta), \dots, \lambda_n(\delta)\}$ , of order  $\mathcal{O}(\delta^{-2})$ . More precisely, there exists  $C_0 > 0$ ,  $\delta_0 > 0$  and  $c(\delta) : (0, \delta_0] \rightarrow (0, C_0]$  with  $\lim_{\delta \rightarrow 0^+} c(\delta) = 0$  so that for any  $\delta \in (0, \delta_0]$  and  $c \in (c(\delta), C_0]$ ,*

$$\sigma(\mathcal{L}_\delta) \cap \{\lambda \in \mathbb{C} \mid \text{Re } \lambda > c\delta^{-2}\} = \{\lambda_1(\delta), \lambda_2(\delta), \dots, \lambda_n(\delta)\}.$$

Moreover the collision eigenvalues may be labeled so that  $\lambda_j(\delta)$  admits the expansion

$$\lambda_j = v_j\delta^{-2} + \mathcal{O}(\delta^{-1}),$$

where  $v_j$  is the unique positive eigenvalue of the  $j$ -th collision operator  $\mathcal{K}_j$  as defined in [\(3.10\)](#). For the generic case when  $v_i \neq v_j$  for  $i \neq j$ , then  $\mathcal{L}_\delta$  has  $n$  distinctive collision eigenvalues, each of which is simple with the corresponding  $j$ 'th eigenfunction  $\psi_j$  localized on the  $j$ -th collision interval  $K_j(\delta)$  as defined in [\(3.20\)](#). In addition, we have

$$\sigma_{ess}(\mathcal{L}_\delta) = (-\infty, -2], \quad 0 \in \sigma_{pt}(\mathcal{L}_\delta),$$

where, by [Assumption 3.5](#),  $\lambda = 0$  is simple with eigenspace spanned by the translational mode  $\partial_z \phi_{h,\delta}$ .

In [Sect. 4](#) we return to the case of general  $N$  and the general mixing well,  $W$ , and use a formal matched asymptotic expansion to show that the manifold of quasi-bilayers is approximately forward invariant on the  $\mathcal{O}(\varepsilon^{-2})$  time-scales, and derive the evolution of the underlying interface  $\Gamma$  and background state  $\mathbf{m}$ . Compared with the scalar case [\(Dai and Promislow 2013\)](#), the novelty of this derivation lies in the following two points. First, the mFCH equation preserves total mass, but the dressing of an interface  $\Gamma$  with a bilayer profile specifies the total mass, to leading order, as a multiple of

the vector-valued mass per unit area  $\mathbf{M}(\phi_h) \in \mathbb{R}^N$ , see (1.18). Consequently, generic initial data cannot converge to a quasi-bilayer profile if the mass of the initial data is not properly tuned. This effect is manifest in Lemma 4.1, on the  $O(\varepsilon^{-1})$  time scale for initial data which have an  $O(\varepsilon)$  mis-fit with the quasi-bilayer equilibrium—the background state  $\mathbf{m}$  starts at  $O(\varepsilon)$  but converges to  $O(\varepsilon^2)$  on the faster time scale only if the total mass is properly tuned. An analysis of pearling bifurcations for the scalar case shows a sensitivity to the value of the far-field equilibrium, and this is manifested in our numerical investigations, depicted in the right-two panels of Fig. 3. For a mixture of two lipid types and a solvent, initial data that is off by  $O(\varepsilon)$  from the target ratio corresponding to the bilayer leads to a pearling bifurcation in the inner (respectively outer) layer of the bilayer depending upon the nature of the mis-match between initial and target mass vectors. Lemma 4.1 shows that for initial composition corresponding to a multiple of the bilayer mass vector, the far-field equilibrium  $\mathbf{m}$  tends to  $O(\varepsilon^2)$  on the fast  $O(\varepsilon^{-1})$  time-scale. Subsequently we enter a slow evolution on the  $O(\varepsilon^{-2})$  time-scale corresponding to an area-preserving Willmore geometric flow, with the far-field state algebraically slaved to enforce conservation of total mass of each species. The second novelty resides in the appearance of the intrinsic curvature in the Willmore formulation of the slow-time geometric flow. More specifically, noting that the generalized mean curvature of the interface admits the expansion  $H(z, s, \tau; \varepsilon) = H_0 + \varepsilon H_1 + O(\varepsilon^2)$  and introducing respectively the squared bilayer mass and the curvature-weighted projection

$$M_2 := \int_{\mathbb{R}} |\phi_h(z)|^2 dz, \quad \Pi_{\Gamma}(f) := f - H_0 \frac{\int_S f H_0 dS}{\int_S H_0^2 dS}, \tag{1.25}$$

we use the method of multiple scales to establish the following formal result.

**Formal Result 1** *For small  $\varepsilon > 0$ , the method of matched asymptotics applied to the  $H^{-1}$  gradient flow of the mFCH free energy shows that in the slow time scale  $\tau_2 = \varepsilon^2 t$ , a quasi-bilayer  $\mathbf{u}_q$  associated to  $\{\mathbf{m}_0, \Gamma_0\}$  evolves as a quasi-bilayer plus a small perturbation, that is,*

$$\mathbf{u}(\tau_2, x, \varepsilon) = \mathbf{u}_q(x, \varepsilon; \mathbf{m}(\tau_2), \Gamma(\tau_2)) + \varepsilon^2 \mathbf{u}_p(\tau_2, x, \varepsilon), \tag{1.26}$$

where  $\|\mathbf{u}_p\|_{L^\infty(\Omega)} = O(1)$  and  $\|\mathbf{u}_p\|_{L^1(\Omega)} = O(\varepsilon)$ . More importantly, the evolution reduces to a surface-area-preserving Willmore flow of the interface  $\Gamma(\tau_2)$ , that is, for  $\tau_2 \geq 0$ , the total interfacial surface area  $|\Gamma(\tau_2)|$  equals the initial surface area  $|\Gamma_0|$  to leading order, and the leading order normal velocity  $V_{n,0}$  satisfies

$$V_{n,0}(s, \tau_2) = M_2^{-1} M_1 \Pi_{\Gamma} \left[ \left( \Delta_s - \frac{1}{2} H_0 (H_0 - a_0) - H_1 \right) (H_0 - a_0) \right], \tag{1.27}$$

while the background state  $\mathbf{m}(\tau_2)$  is slave to the Willmore flow via mass conservation

$$\mathbf{m}(\tau_2) \cdot \mathbf{M} = -M_1 \frac{\int_S \left[ -|\nabla_s H_0|^2 + \frac{\eta_1 + \eta_2}{2} H_0^2 - \frac{1}{2} H_0^2 (H_0 - a_0)^2 - H_1 H_0 (H_0 - a_0) \right] dS}{\int_S H_0^2 dS}, \tag{1.28}$$

where the Melnikov parameter  $a_0$  and the bilayer parameter  $M_1$  are defined in (1.15), the mass per unit length  $\mathbf{M}$  is defined in (1.18) and the curvature-weighted projection  $\Pi_\Gamma$  and squared bilayer mass  $M_2$  are defined in (1.25).

Finally, we break Assumption 2.2, and present a Birkhoff billiard potential for which the stable and unstable manifolds associated the origin of (1.12) intersect non-transversely. The result is a one-parameter family of homoclinics  $\Phi_h(\cdot; \mathbf{m}; \theta)$  which are distinct up to translation, see Example 3.4 and the right-most image in Fig. 5. The corresponding linearized operators  $\mathcal{L}_{\delta, \theta}$  possess a two-dimensional kernel spanned by the translational eigenmode and  $\partial_\theta \Phi_h(\cdot; \mathbf{m}; \theta)$ . The higher order kernel suggests a geometric evolution not only of the shape of the underlying interface,  $\Gamma$ , but also a possibility for a continuous evolution of the composition of the underlying bilayer profile,  $\theta = \theta(s, t)$  where  $s$  parameterizes position along the interface  $\Gamma$ . In such a system the geometric and compositional evolution could couple, leading to a model that couples geometric evolution with lipid composition, as depicted in the bottom-left panel of Fig. 1.

## 2 Quasi-bilayers: a reduction to the Canham–Helfrich free energy

The construction of quasi-bilayer profiles starts with a rigorous definition of an admissible interface  $\Gamma$ . Specifically, we assume the interface  $\Gamma$  is a smooth  $d - 1$  dimensional manifold admitting a volume-preserving parameterization,  $\Xi(s) : S \subset \mathbb{R}^{d-1} \rightarrow \mathbb{R}^d$ . For every  $s \in S$  and  $l > 0$ , we can define a whisker  $\omega(s, l)$  based at  $\Xi(s)$ , that is,

$$\omega(s, l) := \left\{ \Xi(s) + \varepsilon z \mathbf{n}(s) \mid |z| \leq \frac{l}{\varepsilon} \right\},$$

where  $\mathbf{n}(s)$  is the outward unit normal vector of the interface  $\Gamma$  at point  $\Xi(s)$  and  $z$  is the  $\varepsilon$ -scaled, signed distance to the interface  $\Gamma$ . We restricted ourselves to interfaces far from self-intersections.

**Definition 2.1** (Admissible interfaces with reach  $l_0$ ) An admissible interface  $\Gamma \subset \mathbb{R}^d$  is a smooth  $d - 1$  dimensional manifold far from self-intersections. More precisely, there exists  $l_0 > 0$  such that

- (i) No two whiskers of length  $6l_0$  intersect, that is,  $\omega(s_1, 3l_0) \cap \omega(s_2, 3l_0) = \emptyset$ , for any  $s_1 \neq s_2 \in S$ .
- (ii) For each  $l \in (0, 3l_0]$  the set

$$\Gamma_l := \bigcup_{s \in S} \omega(s, l),$$

is a neighborhood of the interface  $\Gamma$ .

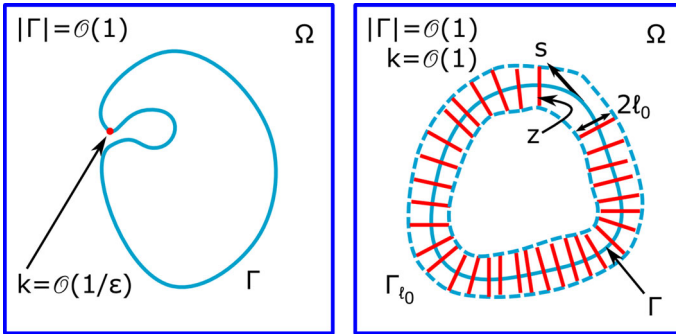


**Fig. 4** In both panels, the *blue rectangle* represents the physical domain  $\Omega$  of the amphiphilic mixture while the *light blue curve* represents the interface  $\Gamma$  of the amphiphilic morphology. The *left panel* shows an inadmissible interface where local whisker coordinates are not well-defined, due to the existence of points (the *red dot*) where the curvature of the interface  $k$  is of order  $\mathcal{O}(1/\varepsilon)$ . The *right panel* depicts an admissible interface  $\Gamma$ : Its length  $|\Gamma|$  is of order  $\mathcal{O}(1)$  and its curvature is of order  $\mathcal{O}(1)$  everywhere. For such an interface, there exists a constant  $l_0 > 0$  such that the union of  $6l_0$ -long whiskers (red lines) form a neighborhood of the interface, depicted as the annulus enclosed by light blue dash curves, denoted by  $\Gamma_{l_0}$ . In addition, no two distinct whiskers of length  $6l_0$  intersect. For an admissible interface the whiskered coordinates  $(z, s)$  give a smooth change of variables of  $\Gamma_{l_0}$ , where  $z$  is the  $\varepsilon$ -scaled signed distance to the interface and  $s$  is the tangential variable of the interface (colour figure online)

We call the set  $\Gamma_{l_0}$  the *inner region* and the set  $\Omega \setminus \Gamma_{l_0}$  the *outer region*, see Fig. 4. In addition, we call  $(z, s) \in [-\frac{l_0}{\varepsilon}, \frac{l_0}{\varepsilon}] \times S \subset \mathbb{R}^d$  the *local whisker coordinates*. The construction of the quasi-bilayer is based on a formal asymptotic analysis in the inner and outer regions; see Fig. 4.

To construct quasi-bilayer solutions of the full PDE (1.11) within the inner region  $\Gamma_{l_0}$ , we derive an ODE system whose homoclinic solutions have sufficient flexibility to approximate the full behavior of the reduction of the PDE to the whiskers. To begin, we transform the stationary mFCH equation (1.11) to the local whiskered coordinates  $(z, s)$ . In the whiskered coordinated the Laplacian becomes

$$\varepsilon^2 \Delta = \partial_z^2 + \varepsilon H(z, s) \partial_z + \varepsilon^2 \Delta_G, \tag{2.1}$$

where at leading order the operator  $\Delta_G$  reduces to the Laplace–Beltrami operator and  $H$  is the extended curvature of the expression,

$$H(z, s) = - \sum_{j=1}^{d-1} \frac{k_j(s)}{1 - \varepsilon r k_j(s)}. \tag{2.2}$$

Here  $\{k_j(s)\}$  is the set of principal curvatures of  $\Gamma$  at  $\Xi(s)$ ; see Doelman et al. (2014) for details about  $H$  and  $\Delta_G$ . We plug the Laplacian (2.1) into the stationary mFCH equation (1.11), yielding,



$$\begin{aligned} & \left( \partial_z^2 + \varepsilon H(z, s) \partial_z + \varepsilon^2 \Delta_G - \nabla_{\mathbf{u}}^2 W(\mathbf{u}) + \varepsilon (\nabla_{\mathbf{u}} \mathbf{V}(\mathbf{u}))^T \right) \\ & \quad \left( \partial_z^2 \mathbf{u} + \varepsilon H(z, s) \partial_z \mathbf{u} + \varepsilon^2 \Delta_G \mathbf{u} - \nabla_{\mathbf{u}} W(\mathbf{u}) + \varepsilon \mathbf{V}(\mathbf{u}) \right) \\ & = \varepsilon^2 \left[ \eta_2 \nabla_{\mathbf{u}} W(\mathbf{u}) - \eta_1 (\partial_z^2 \mathbf{u} + \varepsilon H(z, s) \partial_z \mathbf{u} + \varepsilon^2 \Delta_G \mathbf{u}) + \mathbf{m} \right], \end{aligned} \tag{2.3}$$

which, up to the leading order, reduces to the following ODE system

$$(\partial_z^2 - \nabla_{\mathbf{u}}^2 W(\mathbf{u}))(\partial_z^2 \mathbf{u} - \nabla_{\mathbf{u}} W(\mathbf{u})) = 0.$$

As a starting point in our construction we make the following assumption.

**Assumption 2.2** The leading-order Hamiltonian ODE system (1.12),

$$\partial_z^2 \mathbf{u} - \nabla_{\mathbf{u}} W(\mathbf{u}) = 0,$$

admits, up to translations, an orbit  $\phi_h$  that is homoclinic to the origin. Moreover, the linearized operator

$$\mathcal{L}_0 := \partial_z^2 - \nabla_{\mathbf{u}}^2 W(\phi_h), \tag{2.4}$$

admits 0 as a simple eigenvalue with the corresponding eigenspace spanned by  $\phi'_h(z)$ .

*Remark 2.3* A homoclinic orbit satisfying the condition

$$\int_{\mathbb{R}} \mathbf{V}(\phi_h) \cdot \partial_z \phi_h dz \neq 0. \tag{2.5}$$

is called asymmetric as it cannot have a translate that is even about  $z = 0$ . We will discuss potentials  $W$  which satisfy Assumption 2.2 in Sect. 3.

To develop approximate solutions of (2.3) we assume  $\mathbf{u}$  is independent of  $s$  and replacing the extended curvature  $H$  with a Melnikov parameter  $a$ , yielding the whiskered ODE system,

$$\begin{cases} \partial_z^2 \mathbf{u} + \varepsilon a \partial_z \mathbf{u} - \nabla_{\mathbf{u}} W(\mathbf{u}) + \varepsilon \mathbf{V}(\mathbf{u}) = \varepsilon^2 \mathbf{v}, & (2.6a) \\ (\partial_z^2 + \varepsilon a \partial_z - \nabla_{\mathbf{u}}^2 W(\mathbf{u}) + \varepsilon (\nabla_{\mathbf{u}} \mathbf{V}(\mathbf{u}))^T) \mathbf{v} = \eta_2 \nabla_{\mathbf{u}} W(\mathbf{u}) - \eta_1 (\partial_z^2 \mathbf{u} + \varepsilon a \partial_z \mathbf{u}) + \mathbf{m}. & (2.6b) \end{cases}$$

Assuming  $\mathbf{u}(z) = \phi_h(z) + \mathcal{O}(\varepsilon)$  in (2.6), the leading order term of  $\mathbf{v}$ , denoted  $\zeta_h(z)$ , satisfies the equation,

$$\mathcal{L}_0 \zeta_h(z) = (\eta_2 - \eta_1) \nabla_{\mathbf{u}} W(\phi_h(z)) + \mathbf{m}. \tag{2.7}$$

It is natural to assume  $\zeta_h \perp \ker(\mathcal{L}_0) = \text{span} \{ \partial_z \phi_h \}$  since the projection of  $\zeta_h$  onto the kernel of  $\mathcal{L}_0$  corresponds to a translation of  $\zeta_h$  in  $z$ . With this assumption we have

$$\zeta_h := \mathcal{L}_{0,\perp}^{-1} ((\eta_2 - \eta_1) \nabla_{\mathbf{u}} W(\phi_h) + \mathbf{m}),$$

where  $\mathcal{L}_{0,\perp}^{-1}$  is the bounded inverse of the operator  $\mathcal{L}_0$  restricted to the orthogonal complement of  $\text{span}\{\partial_z \phi_h\}$  in  $(L^2(\mathbb{R}))^N$ . Noting that  $\zeta_h$  converges to a constant state in infinity, that is,

$$\lim_{z \rightarrow \pm\infty} \zeta_h(z) = -(\nabla_{\mathbf{u}}^2 W(0))^{-1} \mathbf{m} := \mathbf{E}$$

Substituting  $\mathbf{E}$  for  $\mathbf{v}$  in (2.6a), yields the whisker ODE system

$$\partial_z^2 \mathbf{u} + \varepsilon a \partial_z \mathbf{u} - \nabla_{\mathbf{u}} W(\mathbf{u}) + \varepsilon \mathbf{V}(\mathbf{u}) = \varepsilon^2 \mathbf{E}, \tag{2.8}$$

which incorporates the Melnikov parameter  $a$  and the far-field parameter  $\mathbf{E}$ . We have the following lemma, which is a special case of the more general Lemma 2.1 in [Homburg and Sandstede \(2010\)](#). We provide a sketch of the proof for our simpler case.

**Lemma 2.4** *Given Assumption 2.2 and any  $\mathbf{m} \in \mathbb{R}^N$ , for sufficiently small  $\varepsilon > 0$ , there exists a unique choice of Melnikov parameter  $a(\varepsilon)$ , in the form of (1.15), for which the whisker ODE system (2.8), admits a homoclinic orbit*

$$\Phi_h(z; \varepsilon) = \phi_h(z) + \mathcal{O}(\varepsilon), \tag{2.9}$$

connecting to the equilibrium

$$\Phi_\infty(\varepsilon) = \varepsilon^2 \mathbf{B} + \mathcal{O}(\varepsilon^3),$$

where the leading-order background state is given by  $\mathbf{B} = (\nabla_{\mathbf{u}}^2 W(0))^{-2} \mathbf{m}$ .

*Proof* To start with, we rewrite the  $2N$ -th-order ODE system (2.8) in first order form, that is,

$$\partial_z \mathbf{U} = F(\mathbf{U}, a, \varepsilon), \tag{2.10}$$

where  $\mathbf{U} := (\mathbf{u}, \mathbf{v})$  and

$$F = \begin{pmatrix} \mathbf{v} \\ \nabla_{\mathbf{u}} W(\mathbf{u}) - \varepsilon \mathbf{V}(\mathbf{u}) - \varepsilon a \mathbf{v} + \varepsilon^2 \mathbf{E} \end{pmatrix}.$$

For  $\varepsilon = 0$ , the ODE system (2.10) reduces to the leading order Hamiltonian ODE (1.12) in its first order form

$$\partial_z \mathbf{U} = \begin{pmatrix} \mathbf{v} \\ \nabla_{\mathbf{u}} W(\mathbf{u}) \end{pmatrix}, \tag{2.11}$$

which, according to Assumption 2.2, admits a homoclinic orbit,  $\mathbf{U}_h(z) := (\phi_h(z), \partial_z \phi_h(z))^T$ , connecting to the hyperbolic equilibrium  $0$ . The persistence of the background equilibrium follows from the hyperbolicity of  $W$  at the origin; given any  $a \in \mathbb{R}$  and sufficiently small  $\varepsilon > 0$ , there exists a hyperbolic equilibrium  $\mathbf{U}_\infty(a, \varepsilon)$  of the ODE (2.10) with the expansion,

$$\mathbf{U}_\infty(a, \varepsilon) = \begin{pmatrix} \varepsilon^2 \mathbf{B} + \mathcal{O}(\varepsilon^3) \\ 0 \end{pmatrix}.$$

The persistence of the homoclinic solution  $\mathbf{U}_h$  of the ODE (2.10) follows via the Melnikov integral method. Linearizing (2.10) at  $\mathbf{U} = \mathbf{U}_h$  when  $\varepsilon = 0$ , yields the system

$$\partial_z \mathbf{U}(z) = \begin{pmatrix} 0 & \mathbf{I}_2 \\ \nabla_{\mathbf{u}}^2 W(\phi_h(z)) & 0 \end{pmatrix} \mathbf{U}(z), \tag{2.12}$$

with the corresponding adjoint ODE system

$$\partial_z \tilde{\mathbf{U}}(z) = - \begin{pmatrix} 0 & \nabla_{\mathbf{u}}^2 W(\phi_h(z)) \\ \mathbf{I}_2 & 0 \end{pmatrix} \tilde{\mathbf{U}}(z), \tag{2.13}$$

Denoting the stable and unstable manifold of the equilibrium  $\mathbf{U}_\infty(a, \varepsilon)$  as  $\mathcal{M}^s(\mathbf{U}_\infty(a, \varepsilon))$ ,  $\mathcal{M}^u(\mathbf{U}_\infty(a, \varepsilon))$  respectively, it is straightforward to see that

$$\begin{aligned} T_{\mathbf{U}_h(z)} \mathcal{M}^s(0) \cap T_{\mathbf{U}_h(z)} \mathcal{M}^u(0) &= \text{span} \{ \partial_z \mathbf{U}_h(z) \}, \\ (T_{\mathbf{U}_h(z)} \mathcal{M}^s(0) \oplus T_{\mathbf{U}_h(z)} \mathcal{M}^u(0))^\perp &= \text{span} \{ \mathbf{U}_{ad}(z) \}, \end{aligned} \tag{2.14}$$

where  $\mathbf{U}_{ad}(z) = (-\partial_z^2 \phi_h(z), \partial_z \phi_h(z))^\top$ . Accordingly, we conclude that, for a small open ball  $\mathcal{U}$  centered at  $\mathbf{U}_h(0)$  in the hyperplane  $\mathbf{U}_h(0) + (\text{span} \{ \partial_z \mathbf{U}_h(0) \})^\perp$ , the two  $N$ -dimensional manifolds,

$$\mathcal{U} \cap \left( \mathcal{M}^{s \setminus u}(0) \oplus \text{span} \{ \mathbf{U}_{ad}(0) \} \right),$$

intersect transversally, forming a line,  $\mathbf{U}_h(0) + \text{span} \{ \mathbf{U}_{ad}(0) \}$ . Moreover, the transversal intersection persists as we turn on the  $\varepsilon$ -perturbation, that is, for sufficiently small  $\varepsilon$ , the manifolds  $\mathcal{U} \cap (\mathcal{M}^s(\mathbf{U}_\infty(a, \varepsilon)) \oplus \text{span} \{ \mathbf{U}_{ad}(0) \})$  and  $\mathcal{U} \cap (\mathcal{M}^u(\mathbf{U}_\infty(a, \varepsilon)) \oplus \text{span} \{ \mathbf{U}_{ad}(0) \})$  also intersection transversally, and hence there exist two unique solutions  $\mathbf{U}^s(z; a, \varepsilon)$  defined on  $z \in [0, \infty)$  and  $\mathbf{U}^u(z; a, \varepsilon)$  defined on  $z \in (-\infty, 0]$  of the full system (2.10) such that

$$\mathbf{U}^u(0; a, \varepsilon) - \mathbf{U}^s(0; a, \varepsilon) \in \text{span} \{ \mathbf{U}_{ad}(0) \}.$$

The homoclinic orbit  $\mathbf{U}_h$  persists if  $\mathbf{U}^s(0; a, \varepsilon) = \mathbf{U}^u(0; a, \varepsilon)$  which in light of the relation above is equivalent to the Melnikov condition

$$\mathbf{U}_{ad}(0) \cdot [\mathbf{U}^u(0; a, \varepsilon) - \mathbf{U}^s(0; a, \varepsilon)] = 0. \tag{2.15}$$

The left-hand side of the Melnikov condition admits the Taylor expansion

$$\begin{aligned} &\mathbf{U}_{ad}(0) \cdot [\mathbf{U}^u(0; a, \varepsilon) - \mathbf{U}^s(0; a, \varepsilon)] \\ &= \left[ \int_{\mathbb{R}} \mathbf{U}_{ad}(z) \cdot \partial_\varepsilon F(\mathbf{U}_h(z), 0) dz \right] \varepsilon + \mathcal{O}(\varepsilon^2) \\ &= - \left[ \int_{\mathbb{R}} \partial_z \phi_h(z) \cdot (\mathbf{V}(\phi_h(z)) + a \partial_z \phi_h(z)) dz \right] \varepsilon + \mathcal{O}(\varepsilon^2), \end{aligned}$$

and solving for  $a$  yields the expression (1.15), and the persistence of the homoclinic  $\mathbf{U}_h$  follows.  $\square$

Within the inner region  $\Gamma_{l_0}$ , the quasi-bilayer profile  $\mathbf{u}_q$  equals  $\Phi_h(z; \varepsilon)$ , that is,

$$\mathbf{u}_q(x; \varepsilon) := \Phi_h(z(x); \varepsilon) = \phi_h(z(x)) + \varepsilon\phi_{h,1}(z(x)) + \varepsilon^2\phi_{h,2}(z(x)) + \mathcal{O}(\varepsilon^3), \quad (2.16)$$

where  $x \in \Gamma_{l_0}$  and  $z \in [-l_0/\varepsilon, l_0/\varepsilon]$  and the error terms are comprised of smooth perturbations which are  $\mathcal{O}(\varepsilon^3)$  in the  $L^\infty$  norm. We plug the expansion (2.16) into (2.8) and evaluate its terms of order  $\varepsilon$  and  $\varepsilon^2$ , yielding respectively

$$\begin{cases} \phi_{h,1} = -\mathcal{L}_{0,\perp}^{-1}(\mathbf{V}(\phi_h) + a_0\partial_z\phi_h), \\ \phi_{h,2} = \mathcal{L}_{0,\perp}^{-1}(\zeta_h - a'(0)\partial_z\phi_h - a_0\partial_z\phi_{h,1} + \frac{1}{2}\nabla_{\mathbf{u}}^3W(\phi_h)(\phi_{h,1}, \phi_{h,1}) - \nabla_u\mathbf{V}(\phi_h)\phi_{h,1}). \end{cases}$$

From Lemma 2.4, in the inner region  $\Gamma_{l_0}$ , there exists a constant  $c > 0$  independent of  $\varepsilon$  so that

$$\begin{aligned} \varepsilon^2\Delta\mathbf{u}_q - \nabla_{\mathbf{u}}W(\mathbf{u}_q) + \varepsilon\mathbf{V}(\mathbf{u}_q) &= (\partial_z^2 + \varepsilon H(z, s)\partial_z)\Phi_h - \nabla_{\mathbf{u}}W(\Phi_h) + \varepsilon\mathbf{V}(\Phi_h) \\ &= \varepsilon(H(z, s) - a(\varepsilon))\partial_z\Phi_h + \varepsilon^2\mathbf{E} + \mathcal{O}(\varepsilon^3) \\ &= \varepsilon(H_0(s) - a_0)\partial_z\phi_h + \varepsilon^2\mathbf{E} + \mathcal{O}(\varepsilon^2e^{-c|z|} + \varepsilon^3), \end{aligned}$$

and

$$\begin{aligned} \frac{1}{2}\varepsilon^2\eta_1|\nabla\mathbf{u}_q|^2 + \eta_2W(\mathbf{u}_q) &= \frac{1}{2}\eta_1|\partial_z\Phi_h|^2 + \eta_2W(\Phi_h) \\ &= \frac{1}{2}(\eta_1 + \eta_2)|\partial_z\phi_h|^2 + \mathcal{O}(\varepsilon e^{-c|z|} + \varepsilon^2), \end{aligned}$$

where  $H(z, s) = H_0(s) + \varepsilon zH_1(s) + \mathcal{O}(\varepsilon^2)$ , all the error estimates are in the  $L^\infty$  norm and in the second estimate, we apply the fact that  $\frac{1}{2}|\partial_z\phi_h|^2 = W(\phi_h)$  for all  $z \in \mathbb{R}$ . The Jacobian  $J$  of the change of coordinates from  $x$  into  $(z, s)$  admits the expansion

$$J(z, s) = \varepsilon + \varepsilon^2zH_0(s) + \mathcal{O}(\varepsilon^3); \quad (2.17)$$

see the appendix of Hayrapetyan and Promislow (2014). Applying the two estimates above, we evaluate the mFCH free energy evaluated at  $\mathbf{u}_q$  restricted to  $\Gamma_{l_0}$ , obtaining

$$\begin{aligned}
 \mathcal{F}_{M,inner}(\mathbf{u}_q) &:= \int_{\Gamma_{l_0}} \frac{1}{2} |\varepsilon^2 \Delta \mathbf{u}_q - \nabla_{\mathbf{u}} W(\mathbf{u}_q) + \varepsilon \mathbf{V}(\mathbf{u}_q)|^2 \\
 &\quad - \varepsilon^2 \left( \frac{1}{2} \varepsilon^2 \eta_1 |\nabla \mathbf{u}_q|^2 + \eta_2 W(\mathbf{u}_q) \right) dx \\
 &= \varepsilon^3 \int_S \int_{-l_0/\varepsilon}^{l_0/\varepsilon} \left[ \frac{1}{2} |(H_0(s) - a_0) \partial_z \phi_h + \varepsilon \mathbf{E}|^2 \right. \\
 &\quad \left. - \frac{1}{2} (\eta_1 + \eta_2) |\partial_z \phi_h(z)|^2 \right] dz dS + \mathcal{O}(\varepsilon^4) \\
 &= \frac{1}{2} \varepsilon^3 M_1 \int_S \left[ (H_0(s) - a_0)^2 - (\eta_1 + \eta_2) \right] dS + \mathcal{O}(\varepsilon^4). \tag{2.18}
 \end{aligned}$$

In the last step, we use the fact that

$$\int_{\mathbb{R}} \partial_z \phi_h(z) \cdot \mathbf{E} dz = 0, \quad \int_{-l_0/\varepsilon}^{l_0/\varepsilon} e^{-cz} dz = \mathcal{O}(1), \quad \int_{-l_0/\varepsilon}^{l_0/\varepsilon} 1 dz = \mathcal{O}(\varepsilon^{-1}).$$

The total mass vector of amphiphiles within the inner region  $\Gamma_{l_0}$ , denoted  $\mathcal{M}_{inner}$ , admits the expansion

$$\begin{aligned}
 \mathcal{M}_{inner}(\mathbf{u}_q) &:= \int_{\Gamma_{l_0}} \mathbf{u}_q dx = \varepsilon \int_S \int_{-l_0/\varepsilon}^{l_0/\varepsilon} \Phi_h(z; \varepsilon) \left( 1 + \varepsilon z H_0(s) + \mathcal{O}(\varepsilon^2) \right) dz dS \\
 &= \varepsilon \int_S 1 dS \int_{-l_0/\varepsilon}^{l_0/\varepsilon} (\phi_h(z) + \varepsilon \phi_{h,1}(z) + \varepsilon^2 \mathbf{B}) dz \\
 &\quad + \varepsilon^2 \int_S H_0(s) dS \int_{\mathbb{R}} z \phi_h(z) dz + \mathcal{O}(\varepsilon^3) \\
 &= \varepsilon |\Gamma| \int_{\mathbb{R}} \phi_h(z) dz + \varepsilon^2 \left[ |\Gamma| \left( 2l_0 \mathbf{B} + \int_{\mathbb{R}} \phi_{h,1}(z) dz \right) \right. \\
 &\quad \left. + \int_S H_0(s) dS \int_{\mathbb{R}} z \phi_h(z) dz \right] + \mathcal{O}(\varepsilon^3), \tag{2.19}
 \end{aligned}$$

where we use the fact that the area of  $\Gamma$  and  $S$  are the same, i.e.,  $|\Gamma| = |S|$ .

Within the outer region  $\Omega \setminus \Gamma_{l_0}$ , the quasi-bilayer profile  $\mathbf{u}_q$  makes a smooth transition to the asymptotic state of  $\Phi_{\infty}(\varepsilon, \mathbf{m})$  as specified in (1.16). In particular for any  $x \in \Omega \setminus \Gamma_{l_0}$  we have the estimate,

$$\mathbf{u}_q(x) = \Phi_{\infty}(\varepsilon) + \mathcal{O}(e^{-c/\varepsilon}) = \varepsilon^2 \mathbf{B} + \mathcal{O}(\varepsilon^3). \tag{2.20}$$

With these estimates we find that the outer region contribution to the mFCH free energy and the total mass vector of  $\mathbf{u}_q$  are, respectively,

$$\begin{aligned}
 \mathcal{F}_{M,outer}(\mathbf{u}_q) &:= \int_{\Omega \setminus \Gamma_{l_0}} \frac{1}{2} |\varepsilon^2 \Delta \mathbf{u}_q - \nabla_{\mathbf{u}} W(\mathbf{u}_q) + \varepsilon \mathbf{V}(\mathbf{u}_q)|^2 \\
 &\quad - \varepsilon^2 \left( \frac{1}{2} \varepsilon^2 \eta_1 |\nabla \mathbf{u}_q|^2 + \eta_2 W(\mathbf{u}_q) \right) dx \\
 &= (|\Omega| - 2l_0|\Gamma|) \left[ \frac{1}{2} | - \nabla_{\mathbf{u}} W(\Phi_\infty) + \varepsilon \mathbf{V}(\Phi_\infty) |^2 \right. \\
 &\quad \left. - \varepsilon^2 \eta_2 W(\Phi_\infty) \right] + \mathcal{O}(e^{-c/\varepsilon}) \\
 &= \mathcal{O}(\varepsilon^4), \\
 \mathcal{M}_{outer}(\mathbf{u}_q) &:= \int_{\Omega \setminus \Gamma_{l_0}} \mathbf{u}_q dx = \varepsilon^2 (|\Omega| - 2l_0|\Gamma|) \mathbf{B} + \mathcal{O}(\varepsilon^3). \tag{2.21}
 \end{aligned}$$

has mFCH free energy  $\mathcal{F}_M(\mathbf{u}_q) = \mathcal{F}_{M,inner}(\mathbf{u}_q) + \mathcal{F}_{M,outer}(\mathbf{u}_q)$  and  $\varepsilon$ -scaled total mass vector  $\mathcal{M}(\mathbf{u}_q) = \frac{1}{\varepsilon} (\mathcal{M}_{inner}(\mathbf{u}_q) + \mathcal{M}_{outer}(\mathbf{u}_q))$  which admit the following expansions

$$\begin{cases} \mathcal{F}_M(\mathbf{u}_q) = \varepsilon^3 \frac{M_1}{2} \int_S [(H_0(s) - a_0)^2 - (\eta_1 + \eta_2)] dS + \mathcal{O}(\varepsilon^4), \\ \mathcal{M}(\mathbf{u}_q) = |\Gamma| \int_{\mathbb{R}} \phi_h(z) dz \\ \quad + \varepsilon [|\Omega| \mathbf{B} + |\Gamma| \int_{\mathbb{R}} \phi_{h,1}(z) dz + \int_S H_0(s) dS \int_{\mathbb{R}} z \phi_h(z) dz] + \mathcal{O}(\varepsilon^2). \end{cases}$$

These results establish Theorem 1.

### 3 Regularized-billiard potentials: existence of homoclinics

In this section, we restrict our attention to the case  $N = 2$  and introduce the Birkhoff-billiard potentials,  $B : \mathbb{R}^2 \mapsto \mathbb{R}$ , and their regularized forms, denoted by  $\{B_\delta\}$ , where  $\delta > 0$  is a small free parameter independent of  $\varepsilon$ . We construct  $n$ -collision homoclinic orbits,  $\psi$ , of the Birkhoff–Hamiltonian ODE

$$\partial_z^2 \mathbf{u} - \nabla_{\mathbf{u}} B(\mathbf{u}) = 0, \tag{3.1}$$

and demonstrate their persistence under the regularization, yielding a homoclinic solution  $\psi_\delta$  of

$$\partial_z^2 \mathbf{u} - \nabla_{\mathbf{u}} B_\delta(\mathbf{u}) = 0, \tag{3.2}$$

that satisfies Assumption 2.2. We perform a spectral analysis of the associated linearized operator

$$\mathcal{L}_\delta = \partial_z^2 - \nabla_{\mathbf{u}}^2 B_\delta(\psi_\delta), \tag{3.3}$$

showing that each collision corresponding to a collision eigenvalue—a positive, order of  $\delta^{-2}$  eigenvalue of  $\mathcal{L}_\delta$ . While the essential spectrum of  $\mathcal{L}_\delta$  is uniformly in the left-half complex plane, we give an example of a problem with hidden symmetries that generate a non-trivial kernel, in addition to the translational symmetry of the orbit  $\psi_\delta$ , which leads to novel center-stable modes other than the meandering mode.

### 3.1 Singular Hamiltonian: homoclinics in a billiard limit potential

The Birkhoff-billiard potential is defined as follows.

**Definition 3.1** A map  $B : \mathbb{R}^2 \mapsto \mathbb{R}$  defined on the physical domain,

$$\Sigma := \{\mathbf{u} \in \mathbb{R}^2 \mid u_1 + u_2 \leq 1, u_1, u_2 \geq 0\},$$

is a **Birkhoff billiard potential**, if it satisfies the following conditions.

- (i) There exists  $R_0 \in (0, 1)$  such that the potential  $B(\mathbf{u})$  is radially symmetric in  $\mathbf{u}$  on the quadrant  $\mathcal{Q} := \{\mathbf{u} \in \Sigma \mid |\mathbf{u}| < R_0\}$ . In addition, there exists an integer  $\ell \geq 2$ , a positive constant  $b^+$  and a strictly increasing  $C^{\ell+1}$ -smooth function  $b(r)$  defined on  $[0, R_0]$  with

$$b(r) = \begin{cases} r^2, & r \in [0, R_0/3], \\ b^+, & r = R_0, \end{cases}$$

so that  $B(\mathbf{u}) = b(|\mathbf{u}|)$ , for  $\mathbf{u} \in \mathcal{Q}$ .

- (ii) The potential  $B(\mathbf{u})$  is piecewise constant on the **billiard region**  $\mathcal{B} := \Sigma \setminus \mathcal{Q}$ . More specifically, there exist two mutually disjoint simply connected open sets  $\mathcal{B}^\pm \subset \mathcal{B}$  with  $\mathcal{B} = \overline{\mathcal{B}^+} \cup \overline{\mathcal{B}^-}$  such that

$$B(\mathbf{u}) = \begin{cases} b_+, & \mathbf{u} \in \overline{\mathcal{B}^+}, \\ -b_-, & \mathbf{u} \in \overline{\mathcal{B}^-}. \end{cases} \tag{3.4}$$

In addition, the potential  $B(\mathbf{u})$  is  $C^{\ell+1}$ -smooth in the simply connected domain  $\Sigma \setminus \mathcal{B}^-$  and the common boundary, called the *collision curve*,  $\mathcal{A} := \overline{\mathcal{B}^+} \cap \overline{\mathcal{B}^-}$  is  $C^{\ell+1}$ -smooth with positive length. There also exists a neighborhood of  $\mathcal{A}$  in the physical domain  $\Sigma$ , denoted as  $\mathcal{N}(\mathcal{A})$ , and a  $C^{\ell+1}$ -smooth signed distance function  $\rho(\mathbf{u})$  defined on  $\mathcal{N}(\mathcal{A})$  such that

$$\rho(\mathbf{u}) \big|_{\mathbf{u} \in \mathcal{B}^+ \cap \mathcal{N}(\mathcal{A})} > 0, \quad \nabla_{\mathbf{u}} \rho(\mathbf{u}) \big|_{\mathbf{u} \in \mathcal{N}(\mathcal{A})} \neq 0,$$

and the collision curve  $\mathcal{A}$  is the zero level set of  $\rho(\mathbf{u})$ , that is,

$$\mathcal{A} \subseteq \{\mathbf{u} \in \mathcal{N}(\mathcal{A}) \mid \rho(\mathbf{u}) = 0\}.$$

We study the leading-order Hamiltonian ODE system (3.1) which we rewrite as a first-order system,

$$\partial_z \begin{pmatrix} \mathbf{u} \\ \mathbf{v} \end{pmatrix} = \begin{pmatrix} \mathbf{v} \\ \nabla_{\mathbf{u}} B(\mathbf{u}) \end{pmatrix}, \tag{3.5}$$

with the Hamiltonian  $H(\mathbf{U}) = \frac{1}{2}|\mathbf{v}|^2 - B(\mathbf{u})$  where  $\mathbf{U} := (\mathbf{u}, \mathbf{v})^T$ . For clarity, we use the term *orbit* for an orbit in the phase space and the term *trajectory* for the projection of an orbit onto the  $\mathbf{u}$ -plane. A point  $\mathbf{U} = (\mathbf{u}, \mathbf{v})^T$  in the phase space is called an *inner*

point if  $\mathbf{u} \in \mathcal{B}^+$  and a collision point if  $\mathbf{u} \in \mathcal{A} \cap \mathcal{B}^o$ . At the moment of a collision, say  $z$ , the flow of (3.5) satisfies the reflection law, that is, the angle of incidence equals the angle of reflection, or more precisely,

$$\mathbf{n} \cdot (\mathbf{v}_+(z) + \mathbf{v}_-(z)) = 0, \quad \mathbf{v}_+(z) - \mathbf{v}_-(z) = [\mathbf{n} \cdot (\mathbf{v}_+(z) + \mathbf{v}_-(z))] \mathbf{n}, \quad (3.6)$$

where  $\mathbf{v}_\pm(z) := \lim_{s \rightarrow z^\pm} \mathbf{v}(s)$  and  $\mathbf{n}$  is the unit normal vector of the collision curve  $\mathcal{A}$  at point  $\mathbf{u}(z)$ .

*Remark 3.2* The Birkhoff-billiard potentials have been studied when the collision curve  $\mathcal{A}$  is piecewise smooth, however the reflection law fails when the normal vector is not well-defined. Such a collision is generically not well-defined unless the billiard region  $\mathcal{B}^+$  is a fundamental domain of a finite Coxeter group, see Kozlov and Treshchëv (1991) for details.

Our assumption that the origin  $\mathbf{u} = 0$  is a strict local minimum point of  $B(\mathbf{u})$  indicates that the origin is an equilibrium for the Hamiltonian ODE (3.5), admitting a two dimensional stable manifold,  $\mathcal{M}^s(0)$ , and a two dimensional unstable manifold,  $\mathcal{M}^u(0)$ . While  $\mathcal{M}^s(0)$  and  $\mathcal{M}^u(0)$  lie in the three dimensional invariant manifold  $\mathcal{H}_0 := \{\mathbf{U} \in \mathbb{R}^4 \mid H(\mathbf{U}) = 0\}$ , the conditions of Definition 3.1 are not sufficient to conclude that the intersection  $\mathcal{M}^s(0) \cap \mathcal{M}^u(0)$  gives an orbit homoclinic to the origin. We introduce two main assumptions—the existence and transversality of a homoclinic orbit.

**Assumption 3.3** (*Existence of a homoclinic orbit*) There exists  $n \in \mathbb{Z}^+$  and  $z_1 < z_2 < \dots < z_n$  such that the Hamiltonian system (3.5),

$$\partial_z \begin{pmatrix} \mathbf{u} \\ \mathbf{v} \end{pmatrix} = \begin{pmatrix} \mathbf{v} \\ \nabla_{\mathbf{u}} B(\mathbf{u}) \end{pmatrix},$$

with a billiard potential  $B(\mathbf{u})$  admits an  $n$ -collision orbit homoclinic to the origin, denoted by  $\Psi_h(z) = (\psi_h(z), \partial_z \psi_h(z))^T$ , satisfying that

$$\left\{ \begin{array}{l} n\text{-collision} : \{z \in \mathbb{R} \mid \psi_h(z) \in \mathcal{A}\} = \{z_i\}_{i=1}^n \subset \mathcal{B}^o, \end{array} \right. \quad (3.7a)$$

$$\left\{ \begin{array}{l} \text{Piecewise-linearity} : \{\psi_h(z) \mid z \in (z_i, z_{i+1})\} \subset \mathcal{B}^+, i = 1, 2, \dots, n - 1, \end{array} \right. \quad (3.7b)$$

$$\left\{ \begin{array}{l} \text{Non-tangency} : \mathbf{n}_i \cdot \partial_z \psi_h(z_i) \neq 0, i = 1, 2, \dots, n, \end{array} \right. \quad (3.7c)$$

where  $\mathbf{n}_i$  is the unit normal vector of  $\mathcal{A}$  at the  $i$ -th collision point  $\mathbf{c}_i := \psi_h(z_i)$  for all  $i$ . Without loss of generality, we set  $z_1 = 0$ .

The condition (3.7a) implies that the homoclinic trajectory intersect the collision curve  $\mathcal{A}$  precisely  $n$  distinct moments, but not necessarily  $n$  distinct points; see Fig. 5. The condition (3.7b) requires the homoclinic orbit does not leave  $\mathcal{B}_+$  between collisions, and hence the orbit is piecewise linear between collisions. The condition (3.7c) guarantees that the collisions are *not tangential*: a tangential collision,  $\mathbf{n}_i \cdot \partial_z \psi_h(z_i) = 0$ , leads to a degeneracy—a loss of the smoothness of the flow



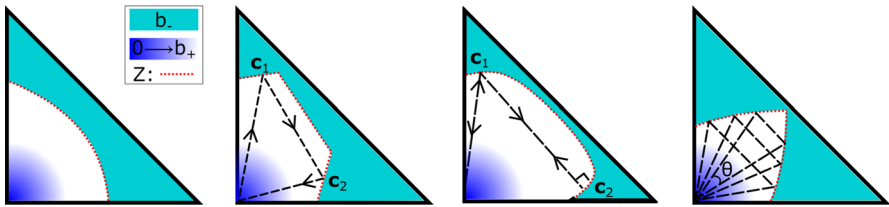


**Fig. 5** In each panel, the *triangle* denotes the physical domain  $\Sigma$ , the potential is positive by smaller than  $b^+$  in the faded blue region, the white region is  $\mathcal{B}^+$ , the cyan region is  $\mathcal{B}^-$ , the *red dotted line* in-between is the collision curve,  $\mathcal{A}$ , while the *black dashed lines* denote trajectories of a homoclinic orbit. The leftmost panel gives a billiard potential. The middle two panels present a 2-collision homoclinic (*middle left*) and a 3-collision homoclinic (*middle right*), both admitting two distinct collision points. The middle left panel presents a billiard potential satisfying both Assumptions 3.3 and 3.5. The rightmost panel is a *universal billiard* potential which admits a family of homoclinics parameterized by the angle  $\theta$ . This potential shows that symmetries other than translation may exist; see Example 3.4 for more details (colour figure online)

and a generic failure of the persistence of the homoclinic orbit with respect to perturbations, see Rapoport et al. (2007) for details about degenerate collisions. Figure 5 presents two generic cases with direct physical interpretations: a 2-collision homoclinic orbit (*middle left panel*) corresponds to an asymmetric *AB*-type bilayer, and a 3-collision homoclinic with 2 distinct collision points (*middle right panel*) corresponding to a symmetric *ABA*-type bilayer, where *A* and *B* are the phase of two distinctive amphiphilies, see also Fig. 2.

Assumption 3.3 can be readily satisfied by a straightforward tuning of the collision curve  $\mathcal{A}$ , but not all homoclinics persist under smooth perturbations of the billiard potential. The following is an important class of counterexample that admits a one parameter family of co-existing homoclinics.

*Example 3.4* (A universal Birkhoff-billiard potential) For any fixed  $c \in (\frac{1}{2}, \frac{7}{8}]$ , we define the universal billiard potential,

$$\Theta_c(\mathbf{u}) = \begin{cases} |\mathbf{u}|^2, & |\mathbf{u}| \leq 1/4, \\ \frac{1}{4}, & \mathbf{u} \in \left\{ \mathbf{u} \in \Sigma \mid |\mathbf{u}| + \frac{1}{\sqrt{2}}|u_1 - u_2| \leq c, |\mathbf{u}| > \frac{1}{2} \right\}, \\ -\frac{1}{4}, & \mathbf{u} \in \left\{ \mathbf{u} \in \Sigma \mid |\mathbf{u}| + \frac{1}{\sqrt{2}}|u_1 - u_2| > c, |\mathbf{u}| > \frac{1}{2} \right\}, \end{cases}$$

yielding, up to translation, a family of homoclinic orbits connecting the origin, parameterized by the angle  $\theta$  of the homoclinic trajectory formed at the origin; see the rightmost panel of Fig. 5. We anticipate the existence of a smoothing of the universal billiard potential, denoted as  $\Theta_{c,\delta}$  which preserves a large part of the family of homoclinics. As a result, the dimension of the kernel of the linearized operator  $\mathcal{L}_\delta := \partial_z^2 - \nabla_{\mathbf{u}}^2 \Theta_{c,\delta}$  will be larger than one.

In order to guarantee the persistence of homoclinic orbits under smooth perturbations of the potential, we impose the following transversality assumption.

**Assumption 3.5** (*Transversality of the homoclinic orbit*) The homoclinic orbit  $\Psi_h$  of the ODE (3.5) comprises the transversal intersection of the stable and unstable manifold of the origin, that is, for all  $z \in \mathbb{R}$ ,

$$\mathbf{T}_{\Psi_h(z)\cdot\mathcal{M}^s}(0) \cap \mathbf{T}_{\Psi_h(z)\cdot\mathcal{M}^u}(0) = \text{span} \{ \Psi'_h(z) \},$$

where  $\mathbf{T}_{\mathbf{p}}\mathcal{M}$  represents the tangential space of the point  $\mathbf{p}$  in the manifold  $\mathcal{M}$ .

*Remark 3.6* The set of billiard potentials satisfying Assumptions 3.3 and 3.5 is not empty. In fact, families of such potentials can be readily constructed by straightforward ray-tracing: Given arbitrary two distinctive points  $\mathbf{c}_1, \mathbf{c}_2 \in \Sigma \setminus \{0\}$ , we can tune the boundary  $\mathcal{A}$  according to the reflection law (3.6) so that the triangle with its vertex  $\mathbf{c}_1, \mathbf{c}_2$  and the origin is a unique trajectory of the ODE (3.5) that is homoclinic to the origin; see the middle left panel of Fig. 5.

### 3.2 Nonsingular Hamiltonian: homoclinics in a regularized-billiard potential

The homoclinic orbit in the Birkhoff-billiard potential is singular in the sense that its first derivative admits a jump at each collision due to the reflection law. Being continuous but not  $C^\ell$ -smooth for any  $\ell > 0$  makes linearization difficult. Consequently we introduce the *regularized Birkhoff-billiard potential*, whose dynamics retains the major features of non-smooth Birkhoff-billiard system. In this sub-section we establish the persistence of transverse homoclinic orbits under the regularization. The dynamics away from the collision curve  $\mathcal{A}$  are smooth and easy to manipulate; the delicate part is to smoothen the billiard potential near the boundary  $\mathcal{A}$  while qualitatively minimizing the change of the dynamics nearby.

To introduce regularized-billiard potentials, we define a smooth jump function  $\tilde{\chi}_\delta(\rho) := (\tilde{\chi} * h_\delta)(\rho)$ , where

$$\tilde{\chi}(\rho) = \begin{cases} b_+, & \rho \geq 0, \\ -b_-, & \rho < 0. \end{cases}$$

and  $h$  is the classical mollifier with  $h_\delta(\rho) := \delta^{-1}h(\delta^{-1}\rho)$  for  $\delta > 0$ . There exists  $\delta_0 > 0$  so that  $[-\delta_0, \delta_0]$  is part of the range of  $\rho$ . For any  $\delta \in [-\delta_0, \delta_0]$ , we introduce the *smooth region*

$$\mathcal{N}_\delta(\mathcal{A}) := \{ \mathbf{u} \in \mathcal{N}(\mathcal{A}) \mid -\delta \leq \rho(\mathbf{u}) \leq \delta \}.$$

and the regularized Birkhoff-billiard potential and refer to [Turaev and Rom-Kedar \(1998\)](#) and [Rapoport et al. \(2007\)](#) for a more general definition.

**Definition 3.7** Given a billiard potential  $B(\mathbf{u})$  and any  $\delta \in (0, \delta_0]$ , the potential

$$B_\delta(\mathbf{u}) = \begin{cases} \tilde{\chi}_\delta(\rho(\mathbf{u})), & \mathbf{u} \in \mathcal{N}_\delta(\mathcal{A}), \\ B(\mathbf{u}), & \mathbf{u} \notin \mathcal{N}_\delta(\mathcal{A}). \end{cases} \tag{3.8}$$

is a regularized-billiard potential with respect to the billiard potential  $B(\mathbf{u})$ .

Replacing the Birkhoff-billiard potential with the regularization yields a smooth Hamiltonian system

$$\begin{pmatrix} \dot{\mathbf{u}} \\ \dot{\mathbf{v}} \end{pmatrix} = \begin{pmatrix} \mathbf{v} \\ \nabla_{\mathbf{u}} B_{\delta}(\mathbf{u}) \end{pmatrix}, \tag{3.9}$$

with Hamiltonian  $H(\mathbf{U}; \delta) = \frac{1}{2}|\mathbf{v}|^2 - B_{\delta}(\mathbf{u})$ . By Definition 3.7, the origin is again a hyperbolic equilibrium of the system (3.9) admitting a two-dimensional stable manifold,  $\mathcal{M}^s(0; \delta)$ , and a two-dimensional unstable manifold,  $\mathcal{M}^u(0; \delta)$ . We claim that, for sufficiently small  $\delta$ , transverse homoclinic orbits in the limit billiard system (3.5) persist as solutions of (3.9).

**Proposition 3.8** *Given a Birkhoff billiard potential  $B(\mathbf{u})$  for which the ODE (3.5), admits an  $n$ -collision homoclinic  $\Psi_h = (\psi_h, \partial_z \psi_h)^T$  satisfying Assumptions 3.3 and 3.5, then for any sufficiently small  $\delta > 0$ , the regularized-billiard Hamiltonian system (3.9), admits a locally unique orbit  $\Psi_{h,\delta} = (\psi_{h,\delta}, \partial_z \psi_{h,\delta})^T$  homoclinic to zero for which*

$$\lim_{\delta \rightarrow 0^+} \|\Psi_{h,\delta}(z) - \Psi_h(z)\|_{L^\infty} = 0. \tag{3.10}$$

To prove the proposition, we recall a Lemma, which states that restricted to inner points, the smooth regularized-billiard flow, denoted as  $\mathbf{f}_\delta(z, \mathbf{U})$ , converges to the Birkhoff-billiard flow, denoted by  $\mathbf{f}(z, \mathbf{U})$ , in the  $C^\ell$ -topology, as  $\delta \rightarrow 0^+$ . We use the notation  $\mathbf{f}_0(z, \mathbf{U}) = \mathbf{f}(z, \mathbf{U})$  where convenient.

**Lemma 3.9** (Turaev and Rom-Kedar 1998) *For any inner point  $\mathbf{U}_1$  and any  $z > 0$  so that  $\mathbf{U}_2 := \mathbf{f}(z, \mathbf{U}_1)$  is also an inner point, there exists a neighborhood of  $\mathbf{U}_1 \setminus \mathbf{U}_2$ , denoted as  $\mathcal{N}(\mathbf{U}_1 \setminus \mathbf{U}_2)$ , and an interval containing  $z$ , denoted as  $I$ , so that, for sufficiently small  $\delta > 0$ ,*

$$\|\mathbf{f}_\delta - \mathbf{f}\|_{C^\ell(I \times \mathcal{N}(\mathbf{U}_1), \mathcal{N}(\mathbf{U}_2))} = \mathcal{O}(\delta). \tag{3.11}$$

We refer to Turaev and Rom-Kedar (1998) for the proof of Lemma 3.9 and give the proof of Proposition 3.8 as follows.

*Proof* The idea is to show that the transversality stated in the Assumption 3.5 still holds for the regularized-billiard system (3.9) for  $\delta$  small. We only prove the case when  $n = 2$ . The general proof for  $n \in \mathbb{Z}^+$  is quite similar and thus omitted.

The unperturbed ODE (3.5) is Hamiltonian and thus admits  $\mathcal{H}_0 = \{\mathbf{u} \mid H(\mathbf{u}) = 0\}$  as a three dimensional invariant manifold. For small  $\xi > 0$ , the set

$$\mathcal{S}(\xi) := \{\mathbf{U} \in \mathcal{H}_0 \mid \mathbf{u} \in \mathcal{A}, |\mathbf{U} - \Psi_{h,+}(z_2)| < \xi\},$$

where  $\Psi_{h,+}(z_2) := \lim_{z \rightarrow z_2^+} \Psi_h(z)$ , provides a two dimensional cross section of  $\Psi_h$  in  $\mathcal{H}_0$ . However, the set  $\mathcal{S}(\xi)$  has a drawback: As we perturb  $\delta$  away from 0, the intersections  $\mathcal{S}(\xi) \cap \mathcal{M}^{s \setminus u}(0; \delta)$  can be empty. Instead, we take a cross section close to  $\mathcal{S}(\xi)$ , which accommodates the persistence of the intersection. We choose  $z_0 > 0$  so small that  $\{\psi_h(z) \mid z \in [-z_0, z_2 + z_0] \setminus \{0, z_2\}\} \subset \mathcal{B}^+$  and the set

$$\mathcal{S}_2(\xi) := z_0(\partial_z \psi_h(z_2 + z_0), 0)^T + \mathcal{S}(\xi),$$

is a translation of  $\mathcal{S}(\xi)$  centered at  $\Psi_h(z_2 + z_0)$ , admitting the same transversal property as  $\mathcal{S}(\xi)$ . As a result, we take  $\xi$  so small that  $\mathcal{S}_2(\xi) \cap \mathcal{M}^{s \setminus u}(0)$  is a  $C^\ell$ -smooth curve, denoted as  $\mathbf{G}_{s \setminus u}(y)$ ,  $y \in Y \subset \mathbb{R}$ . From Assumption 3.5 it is true that  $\Psi_h(z_2 + z_0)$  is the only intersection point of two curves  $\mathbf{G}_s$  and  $\mathbf{G}_u$ . Without loss of generality, we assume  $\mathbf{G}_s(0) = \mathbf{G}_u(0) = \Psi_h(z_2 + z_0)$ . Most importantly, the intersection is transversal, or equivalently,  $\mathbf{G}'_s(0)$  and  $\mathbf{G}'_u(0)$  are linearly independent. Since  $\{\psi_h(z) \mid z > z_2\} \cap \mathcal{A} = \emptyset$ , for sufficiently small  $\delta$ , we can parameterize  $\mathcal{M}^s(0; \delta) \cap \mathcal{S}_2(\xi)$  by  $\mathbf{G}_{s,\delta}(t)$ ,  $t \in T$ . Moreover, we have

$$\|\mathbf{G}_{s,\delta} - \mathbf{G}_s\|_{(C^\ell(T))^4} = \mathcal{O}(\delta). \tag{3.12}$$

In order to describe  $\mathcal{M}^u(0; \delta) \cap \mathcal{S}_2(\xi)$ , we introduce a family of *Poincaré maps* to control the flow near the collision curve. Close to the first collision point, we take a two dimensional cross section centered at  $\Psi_h(-z_0)$ ,

$$\mathcal{S}_1(\tilde{\xi}) := \{\mathbf{U} \in \mathcal{H}_0 \mid [\mathbf{U} - \Psi_h(-z_0)] \cdot (\partial_z \psi_h(-z_0), 0)^T = 0, |\mathbf{U} - \Psi_h(-z_0)| < \tilde{\xi}\},$$

where  $\tilde{\xi}$  is sufficiently small so that the  $C^\ell$ -smooth Poincaré map

$$\begin{aligned} \Pi : \mathcal{S}_1(\tilde{\xi}) &\longrightarrow \mathcal{S}_2(\xi) \\ \mathbf{U} &\longmapsto \mathbf{f}(Z(\mathbf{U}), \mathbf{U}), \end{aligned} \tag{3.13}$$

is well defined with  $\Pi(\mathcal{S}_1(\tilde{\xi})) \subset (\mathcal{S}_2(\xi))^o$ . Here  $Z(\mathbf{U}) > 0$  is the  $C^\ell$ -smooth time of first arrival at  $\mathcal{S}_2(\xi)$ . Based on Lemma 3.9 and the definition of  $\Pi$ , there exists  $\tilde{\delta}_0 \in (0, \delta_0)$  so that, for any  $\delta \in [0, \tilde{\delta}_0]$ , the Poincaré map

$$\begin{aligned} \Pi_\delta : \mathcal{S}_1(\tilde{\xi}) &\longrightarrow \mathcal{S}_2(\xi) \\ \mathbf{U} &\longmapsto \mathbf{f}_\delta(Z_\delta(\mathbf{U}), \mathbf{U}), \end{aligned} \tag{3.14}$$

is well-defined with  $\Pi_\delta(\mathcal{S}_1(\tilde{\xi})) \subset (\mathcal{S}_2(\xi))^o$ . We now define  $\tilde{\mathbf{G}}_u(y) := \Pi^{-1}(\mathbf{G}_u(y))$  and thus there exists an interval  $\tilde{Y} \subseteq Y$  such that the  $C^\ell$ -smooth curve  $\tilde{\mathbf{G}}_u(y)$ ,  $y \in \tilde{Y}$ , is the intersection  $\mathcal{W}^u(0) \cap \mathcal{S}_1(\tilde{\xi})$ . Similarly to the case of  $\mathcal{W}^s(0; \delta)$ , for sufficiently small  $\delta$ , the intersection  $\mathcal{W}^u(0; \delta) \cap \mathcal{S}_1$  can be parameterized by  $\tilde{\mathbf{G}}_{u,\delta}(y)$ ,  $y \in \tilde{Y}$ . Moreover, we have

$$\|\tilde{\mathbf{G}}_{u,\delta} - \tilde{\mathbf{G}}_u\|_{(C^\ell(\tilde{Y}))^4} = \mathcal{O}(\delta). \tag{3.15}$$

It is now straightforward to see that  $\mathbf{G}_{u,\delta}(y) := \Pi_\delta(\tilde{\mathbf{G}}_{u,\delta}(y))$  is the parameterization of  $\mathcal{W}^u(0; \delta)$  in  $\Pi_\delta(\mathcal{S}_1(\tilde{\xi})) \subset \mathcal{S}_2(\xi)$ . Furthermore, we have

$$\begin{aligned} \|\mathbf{G}_{u,\delta} - \mathbf{G}_u\|_{(C^\ell(\tilde{Y}))^4} &= \|\Pi_\delta(\tilde{\mathbf{G}}_{u,\delta}) - \Pi(\tilde{\mathbf{G}}_u)\|_{(C^\ell(\tilde{Y}))^4} \\ &\leq \|\Pi_\delta(\tilde{\mathbf{G}}_{u,\delta}) - \Pi(\tilde{\mathbf{G}}_{u,\delta})\|_{(C^\ell(\tilde{Y}))^4} \\ &\quad + \|\Pi(\tilde{\mathbf{G}}_{u,\delta}) - \Pi(\tilde{\mathbf{G}}_u)\|_{(C^\ell(\tilde{Y}))^4}. \end{aligned} \tag{3.16}$$

From Lemma 3.9 it is known that the first term on the right side in (3.16) is of order  $\mathcal{O}(\delta)$  while the estimate (3.15) indicates that the second term on the right side in (3.16)

is also of order  $\mathcal{O}(\delta)$ . As a result, we have

$$\|\mathbf{G}_{u,\delta} - \mathbf{G}_u\|_{(C^\ell(\tilde{Y}))^4} = \mathcal{O}(\delta). \tag{3.17}$$

Combining the estimates (3.12) and (3.17), we conclude that, for sufficiently small  $\delta > 0$ , the manifolds  $\mathcal{S}_1(\xi) \cap \mathcal{M}^{su}(0, \delta)$  intersect transversally at a point. This intersection point corresponds to a homoclinic orbit, denoted as  $\Psi_{h,\delta}$ , converging to  $\Psi_h$  as  $\delta$  goes to zero.  $\square$

### 3.3 Spectral analysis of the linearization: the origin and the collisions

In this sub-section, we analyze the eigenvalue problem associated to the linearization of the regularized Birkhoff-Billiard homoclinics established in Proposition 3.8. More specifically, for  $\psi_{h,\delta}$  the homoclinic associated to the regularized Birkhoff-potential  $B_\delta$ , then the corresponding linearization (1.23) takes the form

$$\mathcal{L}_\delta := \partial_z^2 - \mathbf{H}_\delta(z),$$

where  $\mathbf{H}_\delta(z) := \nabla_{\mathbf{u}}^2 B_\delta(\psi_{h,\delta}(z))$  is the Hessian of  $B_\delta(\mathbf{u})$  with respect to  $\mathbf{u}$  at  $\psi_{h,\delta}(z)$ . The spectrum,  $\sigma(\mathcal{L}_\delta)$ , plays an important role in associated pearling stability of the corresponding quasi-bilayers  $\mathbf{u}_q$  obtained by dressing admissible interfaces with  $\Psi_{h,\delta}(z)$ . The operator  $\mathcal{L}_\delta$  is closed for  $\delta > 0$  but not well-defined for  $\delta = 0$ . For small  $\delta > 0$ , we localize the spectrum of the operator  $\mathcal{L}_\delta$ , which consists of the essential spectrum  $\sigma_{ess}(\mathcal{L}_\delta)$  and the point spectrum  $\sigma_{pt}(\mathcal{L}_\delta)$ .

By the Weyl essential spectrum theorem, see Kapitula and Promislow (2013) and Kato (1976); Reed and Simon (1978), the essential spectrum of  $\sigma_{ess}(\mathcal{L}_\delta)$ , is determined by the behavior of  $B_\delta(\mathbf{u})$  near the *origin*  $\mathbf{u} = 0$ . Since as  $z \rightarrow \pm\infty$ , the symmetric matrix  $\mathbf{H}_\delta(z)$  limits to the constant matrix  $\nabla_{\mathbf{u}}^2 B(0) = 2\mathbf{I}_2$ , independent of the choice of  $\delta$ , we introduce the *asymptotic operator* associated with  $\mathcal{L}_\delta$ ,

$$\begin{aligned} \mathcal{L}_\infty : (H^2(\mathbb{R}))^2 &\longrightarrow (L^2(\mathbb{R}))^2 \\ \mathbf{w} &\longmapsto \partial_z^2 \mathbf{w} - 2\mathbf{w}. \end{aligned} \tag{3.18}$$

It follows that  $\mathcal{L}_\delta - \mathcal{L}_\infty$  is a compact operator and from the Weyl essential spectrum theorem the two operators share the same essential spectrum,

$$\sigma_{ess}(\mathcal{L}_\delta) = \sigma_{ess}(\mathcal{L}_\infty) = (-\infty, -2]. \tag{3.19}$$

The point spectrum of a linear operator is in general more difficult to localize than its essential spectrum; see Kapitula and Promislow (2013). Instead of an exhaustive description of the point spectrum  $\sigma_{pt}(\mathcal{L}_\delta)$ , we characterize the eigenvalues arising from *collisions*, which correspond to the largest eigenvalues in the limit  $\delta \rightarrow 0^+$ .

We start by defining the collision times of perturbed homoclinics. For a perturbed homoclinic trajectory  $\psi_{h,\delta}$  arising from the unperturbed  $n$ -collision homoclinic trajectory  $\psi_h$  as in Proposition 3.8, the set of *collision times* of the homoclinic  $\psi_{h,\delta}$  are defined as

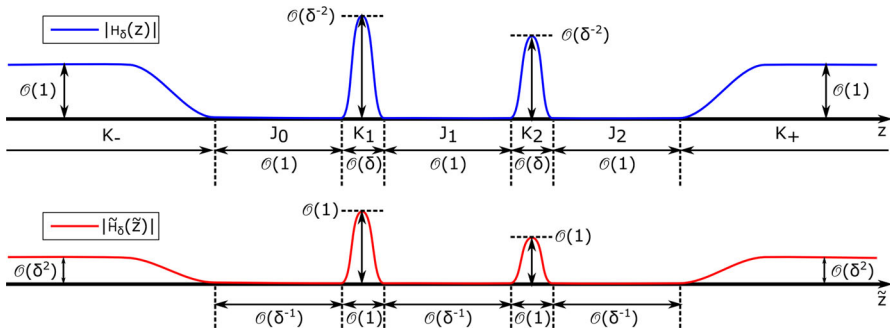


**Fig. 6** The top and bottom panel are respectively cartoon sketches of the profiles  $|\mathbf{H}_\delta|$  and  $|\tilde{\mathbf{H}}_\delta|$

$$\{z \in \mathbb{R} \mid \partial_z \rho(\psi_{h,\delta}(z)) = 0, \psi_{h,\delta}(z) \in \mathcal{N}_\delta(\mathcal{A})\}.$$

This set admits  $n$  elements, denoted as  $\{z_{i,\delta}\}_{i=1}^n$ . For simplicity, we assume  $z_{1,\delta} = 0 < \dots < z_{n,\delta}$ . For a collision time  $z_{i,\delta}$ , the point  $\mathbf{c}_{i,\delta} := \psi_{h,\delta}(z_{i,\delta})$  is the *collision point* and there is a *collision interval*  $K_i(\delta)$  such that  $z_{i,\delta} \in K_i(\delta)$  and

$$\bigcup_{i=1}^n K_i(\delta) = \{z \in \mathbb{R} \mid \psi_{h,\delta}(z) \in \mathcal{N}_\delta(\mathcal{A})\}. \tag{3.20}$$

By definition, we have  $\lim_{\delta \rightarrow 0^+} z_{i,\delta} = z_i$  and  $\lim_{\delta \rightarrow 0^+} \mathbf{c}_{i,\delta} = \mathbf{c}_i$ , where  $\{z_i\}$  and  $\{\mathbf{c}_i\}$  are collision times and points of the unperturbed homoclinic  $\psi_h$ .

To decompose the operator  $\mathcal{L}_\delta$  into a sum of collision operators and asymptotic operators, we chop the real line into  $2n + 3$  intervals; see the top panel of Fig. 6 for an illustration of the case  $n = 2$ . More specifically, we define

$$\begin{cases} Z_-(\delta) := \inf\{z \mid \psi_{h,\delta}(s) \in \mathcal{B}^+, s \in [z, \min\{K_1(\delta)\}]\}, \\ Z_+(\delta) := \sup\{z \mid \psi_{h,\delta}(s) \in \mathcal{B}^+, s \in [\max\{K_n(\delta)\}, z]\}, \end{cases}$$

and

$$\begin{aligned} K_- &:= (-\infty, Z_-], \quad J_0 := (Z_-, \min K_1), \quad J_i := (\max K_i, \min K_{i+1}), \\ J_n &:= (\max K_n, Z_+), \quad K_+ := [Z_+, +\infty), \end{aligned}$$

where  $i = 1, \dots, n - 1$ . As a result, we have

$$\mathbb{R} = \left( \bigcup_{i=1}^n K_i(\delta) \right) \cup \left( \bigcup_{i=\pm} K_i(\delta) \right) \cup \left( \bigcup_{i=0}^{n+1} J_i(\delta) \right). \tag{3.21}$$

Moreover, the length of every  $J_i$  is of order  $\mathcal{O}(1)$ . As for the length of  $K_i$ , by Proposition 3.8, we conclude that, for sufficiently small  $\delta > 0$ ,  $\int_{z \in K_{1 \setminus 2}(\delta)} |\partial_z \psi_{h,\delta}(z)| dz = \mathcal{O}(\delta)$  and  $\min_{z \in K_{1 \setminus 2}(\delta)} |\partial_z \psi_{h,\delta}(z)| = \mathcal{O}(1)$ , yielding

$$|K_i| = \mathcal{O}(\delta), \quad i = 1, \dots, n. \tag{3.22}$$

Let  $\{\kappa_i(z)\}_{i=\pm,1}^n$  be a partition of unity of the real line such that

$$\begin{cases} \sum_{i=\pm,1}^n \kappa_i(z) = 1, & z \in \mathbb{R}, \\ \kappa_i(z) = 1, & z \in K_i(\delta), \quad i = 1, \dots, n, \pm. \end{cases} \tag{3.23}$$

Using such a partition of unity, we define

$$\mathcal{K}_{i,\delta} := \kappa_i \mathcal{L}_\delta, \quad \mathcal{A}_{\pm,\delta} := \kappa_{\pm} \mathcal{L}_\delta. \tag{3.24}$$

and call  $\mathcal{K}_{i,\delta}$  the  $i$ -th collision operator and  $\mathcal{A}_{\pm,\delta}$  the positive/negative asymptotic operator. As a result, we have the decomposition

$$\mathcal{L}_\delta = \mathcal{A}_{-,\delta} + \mathcal{A}_{+,\delta} + \sum_{i=1}^n \mathcal{K}_{i,\delta}. \tag{3.25}$$

In the remainder of this section, we show that for small  $\delta > 0$ , each collision operator admits a positive eigenvalue which persists in the whole linearized operator  $\mathcal{L}_\delta$ . To start, we take a close look at  $\mathbf{H}_\delta(z)$ . A straightforward calculation shows that

$$\mathbf{H}_\delta(z) = \begin{cases} H_1(z; \delta) [\nabla_{\mathbf{u}} \rho(\psi_{h,\delta}(z))]^T \nabla_{\mathbf{u}} \rho(\psi_{h,\delta}(z)) + H_2(z; \delta) \nabla_{\mathbf{u}}^2 \rho(\psi_{h,\delta}(z)), & z \in \bigcup_{i=1}^n K_i(\delta), \\ \nabla_{\mathbf{u}}^2 W(\psi_{h,\delta}(z)), & z \in K_-(\delta) \cup K_+(\delta), \\ 0, & z \in \bigcup_{i=0}^n J_i(\delta), \end{cases} \tag{3.26}$$

where

$$\begin{aligned} H_1(z; \delta) &:= (b_- + b_+) h'_\delta(\rho(\psi_{h,\delta}(z))) = \mathcal{O}(\delta^{-2}), \\ H_2(z; \delta) &:= (b_- + b_+) h_\delta(\rho(\psi_{h,\delta}(z))) = \mathcal{O}(\delta^{-1}). \end{aligned}$$

Since  $\mathbf{H}_\delta = \mathcal{O}(\delta^{-2})$  on the  $\mathcal{O}(\delta)$ -long intervals  $K_i(\delta)$ , there is no obvious well-defined limits for  $\mathcal{L}_\delta$  and  $\mathcal{K}_{i,\delta}$  as  $\delta$  goes to zero. Applying a rescaling  $z = \delta \tilde{z}$  and a  $\delta^2$  scaling to  $\mathcal{L}_\delta$ , we define a rescaled linearized operator

$$\begin{aligned} \tilde{\mathcal{L}}_\delta : (H^2(\mathbb{R}))^2 &\longrightarrow (L^2(\mathbb{R}))^2 \\ \mathbf{w}(\tilde{z}) &\longmapsto \partial_{\tilde{z}}^2 \mathbf{w}(\tilde{z}) - \tilde{\mathbf{H}}_\delta(\tilde{z}) \mathbf{w}(\tilde{z}), \end{aligned} \tag{3.27}$$

where  $\tilde{\mathbf{H}}_\delta(\tilde{z}) := \delta^2 \mathbf{H}_\delta(\delta \tilde{z})$ ; see the bottom panel in Fig. 6 for a scalar description. The sets  $\sigma_{pt}(\tilde{\mathcal{L}}_\delta)$  and  $\sigma_{pt}(\mathcal{L}_\delta)$  are related by the map

$$\sigma_{pt}(\mathcal{L}_\delta) = \delta^{-2} \sigma_{pt}(\tilde{\mathcal{L}}_\delta). \tag{3.28}$$

More specifically, given  $\mathcal{L}_\delta \mathbf{u}(z) = \lambda \mathbf{u}(z)$ , we have  $\tilde{\mathcal{L}}_\delta \mathbf{u}(\delta \tilde{z}) = \delta^2 \lambda \mathbf{u}(\delta \tilde{z})$ . Similarly, we define rescaled collision operators and rescaled asymptotic operators, respectively,

$$\tilde{\mathcal{K}}_{i,\delta}(\tilde{z}) := \kappa_i(\delta \tilde{z}) \tilde{\mathcal{L}}_\delta, \quad \tilde{\mathcal{A}}_{\pm,\delta}(\tilde{z}) := \kappa_\pm(\delta \tilde{z}) \tilde{\mathcal{L}}_\delta,$$

for which the equality  $\tilde{\mathcal{L}}_\delta = \sum_{i=1}^n \tilde{\mathcal{K}}_{i,\delta} + \sum_{j=\pm} \tilde{\mathcal{A}}_{j,\delta}$  holds. More importantly, every rescaled collision operator  $\tilde{\mathcal{K}}_{i,\delta}$ , up to the scaled translation  $\tilde{z} \mapsto \tilde{z} - \delta^{-1} z_{i,\delta}$ , admits a well-defined limit as  $\delta$  goes to zero. In fact, we define the *limit collision operators* as follows.

**Definition 3.10** The  $i$ -th limit collision operator, denoted as  $\mathcal{K}_i$ , is defined as

$$\begin{aligned} \mathcal{K}_i : (H^2(\mathbb{R}))^2 &\longrightarrow (L^2(\mathbb{R}))^2 \\ \mathbf{w}(\tilde{z}) &\longmapsto (\partial_{\tilde{z}}^2 - (b_+ + b_-)h'(Z_i|\tilde{z}|)\nabla_{\mathbf{u}}\rho(\mathbf{c}_i)[\nabla_{\mathbf{u}}\rho(\mathbf{c}_i)]^T)\mathbf{w}(\tilde{z}), \end{aligned} \tag{3.29}$$

where  $Z_i := \mathbf{v}_i \cdot \nabla_{\mathbf{u}}\rho(\mathbf{c}_i)$ ,  $\mathbf{v}_i := (\lim_{z \rightarrow z_i+} \partial_z \psi_h(z) - \lim_{z \rightarrow z_i-} \partial_z \psi_h(z))/2$ , and  $i = 1, \dots, n$ .

We now have the following lemmas.

**Lemma 3.11** For small  $\delta > 0$  and any  $i = 1, \dots, n$ , we have

$$\lim_{\delta \rightarrow 0^+} \|\mathcal{T}_{i,\delta} \circ \tilde{\mathcal{K}}_{i,\delta} - \mathcal{K}_i(\tilde{z})\|_{B([H^2(\mathbb{R})]^2, [L^2(\mathbb{R})]^2)} = 0,$$

where  $(\mathcal{T}_{i,\delta} \mathbf{w})(\tilde{z}) := \mathbf{w}(\tilde{z} + \delta^{-1} z_{i,\delta})$  for any  $\mathbf{w} \in (L^2(\mathbb{R}))^2$ . Moreover, the limit collision operator  $\mathcal{K}_i$  admits a unique positive eigenvalue, denoted  $v_i$ , that is,

$$\sigma(\mathcal{K}_i) \cap \{v \in \mathbb{C} \mid \text{Re } v > 0\} = \{v_i\}.$$

Meanwhile, for small  $\delta > 0$ , there exists  $0 < v_{i,\delta} \in \sigma_{pt}(\tilde{\mathcal{K}}_{i,\delta})$  such that  $v_i = \lim_{\delta \rightarrow 0^+} v_{i,\delta}$  and  $v_{i,\delta}$  is the unique positive eigenvalue of  $\tilde{\mathcal{K}}_{i,\delta}$  with order  $\mathcal{O}(1)$ .

*Proof* We prove the result for the scaled first-collision operator and omit the rest. The truncated first-collision Hessian  $\tilde{\mathbf{H}}_{1,\delta}(\tilde{z}) := \kappa_{1,\delta}(\delta \tilde{z}) \tilde{\mathbf{H}}_\delta(\tilde{z})$  admits the expression

$$\tilde{\mathbf{H}}_{1,\delta}(\tilde{z}) = \begin{cases} \delta^2 \mathbf{H}_\delta(\delta \tilde{z}), & \tilde{z} \in \delta^{-1} \mathcal{K}_{1,\delta}, \\ 0, & \tilde{z} \notin \delta^{-1} \mathcal{K}_{1,\delta}, \end{cases} \tag{3.30}$$

Applying the rescalings  $\rho = \delta \tilde{\rho}$  and  $\mathbf{u} = \mathbf{c}_{1,\delta} + \delta \tilde{\mathbf{u}}$  to the rescaled level-set function  $\tilde{\rho}(\tilde{\mathbf{u}}) := \delta^{-1} \rho(\mathbf{c}_{1,\delta} + \delta \tilde{\mathbf{u}})$ , we have that, for  $\tilde{\psi}_{h,\delta}(\tilde{z}) := \delta^{-1}(\psi_{h,\delta}(\delta \tilde{z}) - \mathbf{c}_{1,\delta})$  and  $\tilde{z} \in \delta^{-1} \mathcal{K}_{1,\delta}$ ,

$$\begin{cases} \nabla_{\mathbf{u}}\rho(\psi_{h,\delta}(z)) = \nabla_{\tilde{\mathbf{u}}}\tilde{\rho}(\tilde{\psi}_{h,\delta}(\tilde{z})) = \nabla_{\mathbf{u}}\rho(\mathbf{c}_1) + \mathcal{O}(\delta), \\ \tilde{\rho}(\tilde{\psi}_{h,\delta}(\tilde{z})) = Z_1|\tilde{z}| + \mathcal{O}(\delta), \\ \delta^2 h'_\delta(\rho(\psi_{h,\delta}(z))) = h'(\tilde{\rho}(\tilde{\psi}_{h,\delta}(\tilde{z}))) = h'(Z_1|\tilde{z}|) + \mathcal{O}(\delta). \end{cases} \tag{3.31}$$



Inserting the expansion (3.31) and the expression (3.26) into (3.30), we obtain

$$\lim_{\delta \rightarrow 0^+} \tilde{\mathbf{H}}_{1,\delta}(\tilde{z}) = (b_+ + b_-)h'(Z_1|\tilde{z})\nabla_{\mathbf{u}}\rho(\mathbf{c}_1)[\nabla_{\mathbf{u}}\rho(\mathbf{c}_1)]^T,$$

implying that  $\lim_{\delta \rightarrow 0^+} \mathcal{K}_{1,\delta} = \mathcal{K}_1$ .

We are left to show that  $\mathcal{K}_1$  admits a positive eigenvalue. Defining

$$\mathbf{n}_1 := \frac{\nabla_{\mathbf{u}}\rho(\mathbf{c}_1)}{\|\nabla_{\mathbf{u}}\rho(\mathbf{c}_1)\|}, \quad \mathbf{t}_1 := \frac{\lim_{z \rightarrow 0^+} \partial_z \psi_h(z) + \lim_{z \rightarrow 0^-} \partial_z \psi_h(z)}{\|\lim_{r \rightarrow 0^+} \partial_z \psi_h(z) + \lim_{r \rightarrow 0^-} \partial_z \psi_h(z)\|}, \quad \mathcal{N}_1 := (\mathbf{n}_1 \ \mathbf{t}_1),$$

we apply the change of coordinates  $\mathbf{w} = \mathcal{N}_1 \tilde{\mathbf{w}}$  to the operator  $\tilde{\mathcal{K}}_{1,\delta}$  to find

$$\mathcal{D}_{1,\delta} := \mathcal{N}_1^{-1} \circ \tilde{\mathcal{K}}_{1,\delta} \circ \mathcal{N}_1 = \begin{pmatrix} \partial_{\tilde{z}}^2 - (b_+ + b_-)h'(Z_1\tilde{z}) & 0 \\ 0 & \partial_{\tilde{z}}^2 \end{pmatrix}.$$

We note that

$$(\partial_{\tilde{z}}^2 - (b_+ + b_-)h'(Z_1\tilde{z}))\tilde{w}_0(\tilde{z}) = 0,$$

where  $\tilde{w}_0(\tilde{z}) := \lim_{\delta \rightarrow 0^+} \mathbf{n}_1 \cdot \partial_z \psi_{h,\delta}(\delta\tilde{z})$  is an increasing function with  $\tilde{w}_0(0) = 0$ . By Sturm-Louville theory, the operator  $\partial_{\tilde{z}}^2 - (b_+ + b_-)h'(Z_1\tilde{z})$ , and thus,  $\mathcal{K}_1$ , admits one and only one positive eigenvalue  $\nu_1$ . The continuation of  $\nu_1$  in  $\tilde{\mathcal{K}}_{1,\delta}$  is a simple classical perturbation argument (Kato 1976), which concludes the proof.  $\square$

**Lemma 3.12** *For small  $\delta > 0$ , the asymptotic operators  $\tilde{\mathcal{A}}_{\pm,\delta}$  have no  $\mathcal{O}(1)$  positive eigenvalues,*

$$\sigma_{pt}(\tilde{\mathcal{A}}_{\pm,\delta}) \cap \{v \in \mathbb{R}^+ \mid v = \mathcal{O}(1)\} = \emptyset.$$

*Proof* We argue by contradiction to show that

$$\sigma_{pt}(\mathcal{A}_{-,\delta}) \cap \{v \in \mathbb{R}^+ \mid v = \mathcal{O}(\delta^{-2})\} = \emptyset.$$

The proof for the operator  $\mathcal{A}_{+,\delta}$  is essentially the same and thus omitted. Due to the radial symmetry of  $B(\mathbf{u})$  near the origin, there exist  $\alpha(\delta) \in [0, \pi/2]$  so that the closure of the trajectory  $\{\psi_{h,\delta}(z) \mid z \in K_-\}$  is a line segment through the origin whose angle with respect to  $u_1$ -axis in the  $\mathbf{u}$ -plane is  $\alpha$ . Consequently, denoting  $\mathbf{t}_- := (\cos(\alpha), \sin(\alpha))^T$ ,  $r(z; \delta) := |\psi_{h,\delta}(z)|$  and  $Z_m(\delta) := \{z \in K_- \mid r(z) = R_0/2\}$ , we have

$$\mathbf{H}_{-,\delta}(z) = \begin{cases} 2\mathbf{I}_2, & z \in (-\infty, Z_m), \\ (b''(r(z)) - b'(r(z))/r(z))\mathbf{t}_-\mathbf{t}_-^T + b'(r(z))/r(z)\mathbf{I}_2, & z \in [Z_m, Z_-], \\ 0, & z \in [Z_-, \infty). \end{cases} \tag{3.32}$$

We denote the  $2 \times 2$  rotation matrix with angle  $\alpha$  as  $\mathcal{N}_-$  and apply the change of coordinates  $\mathbf{w} = \mathcal{N}_- \tilde{\mathbf{w}}$  to the operator  $\mathcal{A}_{-, \delta}$ , yielding

$$\mathcal{D}_{-, \delta} := \mathcal{N}_-^{-1} \circ \mathcal{A}_{-, \delta} \circ \mathcal{N}_- = \begin{pmatrix} \partial_z^2 - b_1(z) & 0 \\ 0 & \partial_z^2 - b_2(z) \end{pmatrix},$$

where

$$b_1(z) = \begin{cases} 2, & z \in (-\infty, Z_m), \\ b''(r(z)), & z \in [Z_m, Z_-], \\ 0, & z \in [Z_-, \infty), \end{cases} \quad b_2(z) = \begin{cases} 2, & z \in (-\infty, Z_m), \\ b'(r(z))/r(z), & z \in [Z_m, Z_-], \\ 0, & z \in [Z_-, \infty). \end{cases}$$

Assume that there exists a positive constant  $v = \mathcal{O}(1)$  so that  $\delta^{-2}v \in \sigma_{pr}(\partial_z^2 - b_1(z))$  with an eigenfunction  $u(z) \in L^2(\mathbb{R})$ , that is,  $\partial_z^2 u(z) - b_1(z)u(z) = \delta^{-2}vu(z)$ . It is then straightforward to see that the *angle function*,  $\beta(z) := \frac{u(z)}{\partial_z u(z)}$ , solves the following second order ODE problem

$$\begin{cases} \partial_z \beta = (\delta^{-2}v + b_1(z)) - \beta^2, & (3.33a) \\ \beta(Z_m) = \sqrt{\delta^{-2}v + 2}, \beta(Z_-) = -\delta^{-1}\sqrt{v}, & (3.33b) \end{cases}$$

which is impossible for sufficiently small  $\delta$ . The reason is quite simple: since  $b_1 = \mathcal{O}(1)$  for all  $z \in \mathbb{R}$ , we have  $\partial_z \beta \gg 1$  when  $\beta = 0$ , which implies that any forward solution of the ODE (3.33a) with positive initial condition will stay positive for all forward time. A similar argument also applies to the operator  $\partial_z^2 - b_2(z)$ . Therefore, the operator  $\mathcal{D}_{-, \delta}$ , thus  $\mathcal{A}_{-, \delta}$ , does not admit any positive eigenvalue of order  $\mathcal{O}(\delta^{-2})$ , which concludes the proof.  $\square$

*Remark 3.13* The reduction to the angle function  $\beta$  is possible only for  $N = 2$ , and in fact is the ‘‘Prüfer transformation’’ that forms the basis of the classical Sturmian theory (Reid 1988). The extension to  $N \geq 2$  requires the use of the Jost matrices of each of the collision operators to expand the Evans function of the full operator, up to exponential corrections, as the product of the Evans functions of the collision operators for the range of  $\lambda$  under consideration. The associated branch point structure of the Jost matrices complicates, but does not fundamentally alter, the nature of the proof, see chapter 10 of Kapitula and Promislow (2013) for details on the Jost matrices.

Having established Lemmas 3.11 and 3.12, we are ready to prove the main theorem of this section.

*Proof of Theorem 2* It remains to prove the statements about the collision eigenvalues. Without loss of generality, we consider only the case  $n = 2$ . Recall that the rescaled linearized operator  $\tilde{\mathcal{L}}_\delta$  admits the decomposition

$$\tilde{\mathcal{L}}_\delta = \tilde{\mathcal{A}}_{-, \delta} + \tilde{\mathcal{K}}_{1, \delta} + \tilde{\mathcal{K}}_{2, \delta} + \tilde{\mathcal{A}}_{+, \delta},$$

where the rescaled collision operator  $\tilde{\mathcal{K}}_{i, \delta}$  admits a positive eigenvalue  $v_{i, \delta} = \mathcal{O}(1)$ , as shown in Lemma 3.11. We restrict ourselves to the continuation of  $v_{1, \delta}$  in  $\tilde{\mathcal{L}}_\delta$ . The

argument is inductive: we first show the continuation of  $v_{1,\delta}$  in  $\tilde{\mathcal{A}}_{-\delta} + \tilde{\mathcal{K}}_{1,\delta}$ , then similar arguments can apply to  $\tilde{\mathcal{A}}_{-\delta} + \tilde{\mathcal{K}}_{1,\delta} + \tilde{\mathcal{K}}_{2,\delta}$  and eventually  $\tilde{\mathcal{L}}_\delta$ . Indeed, the proof boils down to showing the existence of an eigenvalue  $\tilde{\lambda}_{1,\delta} \in \sigma_{pt}(\tilde{\mathcal{K}}_{1,\delta} + \tilde{\mathcal{A}}_{-\delta})$  close to  $v_{1,\delta}$ .

To illustrate the ideas without getting involved in technicalities, we simplify the argument by assuming that  $\tilde{\mathcal{A}}_{-\delta}$  and  $\tilde{\mathcal{K}}_{1,\delta}$  are scalar operators. Defining  $\kappa_1 := \min K_{1,\delta}$ , for  $\tilde{v}$  small, we aim to locate initial conditions  $(d_1(\tilde{v}), d_2(\tilde{v}))$  such that the solution  $(\mathbf{w}(\tilde{z}, d_1, d_2), \partial_{\tilde{z}}\mathbf{w}(\tilde{z}, d_1, d_2))$  of the initial value problem

$$\begin{cases} \tilde{\mathcal{K}}_{1,\delta}\mathbf{w} = (v_{1,\delta} + \tilde{v})\mathbf{w}, \\ \mathbf{w}(\delta^{-1}\kappa_1) = d_1, \\ \partial_{\tilde{z}}\mathbf{w}(\delta^{-1}\kappa_1) = d_2, \end{cases}$$

satisfies

$$\lim_{\tilde{z} \rightarrow +\infty} (\mathbf{w}(\tilde{z}, d_1, d_2), \partial_{\tilde{z}}\mathbf{w}(\tilde{z}, d_1, d_2)) = 0.$$

Since  $v_{1,\delta} \in \sigma_{pt}(\tilde{\mathcal{K}}_{1,\delta})$ , we define

$$(d_1(0), d_2(0)) = (1, \sqrt{v_{1,\delta}}),$$

For  $\tilde{v}$  small, there exists a scalar function  $f(\tilde{v}) = f_0\tilde{v} + \mathcal{O}(\tilde{v}^2)$ ,  $f_0 \neq 0$ , such that

$$(d_1(\tilde{v}), d_2(\tilde{v})) = (1, \sqrt{v_{1,\delta} + \tilde{v}}) + f(\tilde{v})(1, -\sqrt{v_{1,\delta} + \tilde{v}}),$$

The fact that  $f_0 \neq 0$  is a straightforward argument based on Prüfer's substitution (Birkhoff and Rota 1989) and the comparison theorem. Therefore, we have

$$\begin{aligned} & (\mathbf{w}(\delta^{-1}R_-, d_1(\tilde{v}), d_2(\tilde{v})), \partial_{\tilde{z}}\mathbf{w}(\delta^{-1}R_-, d_1(\tilde{v}), d_2(\tilde{v}))) \\ &= e^{\delta^{-1}\sqrt{v_{1,\delta} + \tilde{v}}(R_-\kappa_1)} (1, \sqrt{v_{1,\delta} + \tilde{v}}) + e^{\delta^{-1}\sqrt{v_{1,\delta} + \tilde{v}}(\kappa_1 - R_-)} f(\tilde{v})(1, -\sqrt{v_{1,\delta} + \tilde{v}}). \end{aligned} \tag{3.34}$$

Noting that  $v_{1,\delta} = \mathcal{O}(1)$ , we have

$$\sqrt{v_{1,\delta}}/\delta \gg 1.$$

Therefore, for small  $\delta > 0$ , there always exist  $\tilde{v}_1$  such that the solution to the initial value problem

$$\begin{cases} (\tilde{\mathcal{K}}_{1,\delta} + \mathcal{A}_{-\delta})\mathbf{v} = (v_{1,\delta} + \tilde{v})\mathbf{v}, \\ (\mathbf{v}, \partial_{\tilde{z}}\mathbf{v})(\delta^{-1}R_-, d_1(\tilde{v}), d_2(\tilde{v})) = (\mathbf{w}(\delta^{-1}R_-, d_1(\tilde{v}), d_2(\tilde{v})), \partial_{\tilde{z}}\mathbf{w}(\delta^{-1}R_-, d_1(\tilde{v}), d_2(\tilde{v}))), \end{cases}$$

satisfying

$$\lim_{\tilde{z} \rightarrow -\infty} (\mathbf{v}(\tilde{z}, d_1(\tilde{v}_1), d_2(\tilde{v}_1)), \partial_{\tilde{z}}\mathbf{v}(\tilde{z}, d_1(\tilde{v}_1), d_2(\tilde{v}_1))) = 0.$$

This is precisely what is required for  $\tilde{\lambda}_{1,\delta} = \nu_{1,\delta} + n\tilde{u}_1$  to be an eigenvalue of  $\tilde{\mathcal{K}}_{1,\delta} + \mathcal{A}_{-,\delta}$ , and thus concludes the proof.  $\square$

### 4 Geometric evolution of multi-component bilayers

In this section we return to the general case and analyze the geometric evolution of co-dimensional one quasi-bilayers, deriving their curvature-driven motion under the  $H^{-1}$  gradient flow of the weak mFCH. The results are formal in the sense that we assume the stability of the underlying quasi-bilayers, in particular their stability to the pearling bifurcations described in Sect. 3. Moreover, as is typical in a multi-scale analysis, we assume that the evolution occurs at distinct time scales, which scale according to,

$$\tau_\alpha = \varepsilon^\alpha t, \quad \alpha = -2, -1, 0, 1, 2.$$

More specifically, given a fixed time scale  $\tau_\alpha = \varepsilon^\alpha t$ , we adopt the asymptotic analysis techniques from Dai and Promislow (2013) and Pego (1989) to analyze the initial value problem of the rescaled weak mFCH equation,

$$\varepsilon^\alpha \mathbf{u}_{\tau_\alpha}(x, \tau_\alpha) = \Delta\mu(x, \tau_\alpha), \tag{4.1}$$

subject to initial data that corresponds to the equilibrium of the preceding time-scale. Here the chemical potential  $\mu = \frac{\delta\mathcal{F}_M}{\delta\mathbf{u}}$  and the initial profile is a quasi-bilayer  $\mathbf{u}_q(x, \varepsilon, \mathbf{m}, \Gamma)$  with background state  $\mathbf{m}$  and interface  $\Gamma$ , as defined in (1.16). Since quasi-bilayers are leading order equilibria of (4.1) for  $\alpha \leq 1$ , we first consider the time scale  $\tau_1 = \varepsilon t$ , under a slightly broader class of initial data, called pseudo-bilayers and denoted as  $\mathbf{u}_p(x, \varepsilon; \mathbf{B}, \Gamma)$ , taking the form

$$\mathbf{u}_p(x, \varepsilon; \mathbf{B}, \Gamma) = \begin{cases} \phi_h(z(x)) + \varepsilon(\mathcal{L}_{0,\perp})^{-2}(\mathbf{B} - \mathcal{L}_0\mathbf{V}(\phi_h))(z(x)) + \mathcal{O}(\varepsilon^2), & x \in \Gamma_{l_0}, \\ \varepsilon\mathbf{B} + \mathcal{O}(\varepsilon^2), & x \in \Omega \setminus \Gamma_{3l_0}, \end{cases} \tag{4.2}$$

with a smooth transition in  $\Gamma_{3l_0} \setminus \Gamma_{l_0}$  as in (1.16). Here  $\phi_h$  is an orbit of (1.12) which is homoclinic to the origin, and the pseudo-bilayer reduces to a quasi-bilayer when  $\mathbf{B} = 0$  to leading order. We show that any pseudo-bilayer converges to a quasi-bilayer at leading order as  $\tau_1$  goes to infinity, if and only if the leading order background state  $\mathbf{B}$  is proportional to the quasi-bilayer mass vector  $\mathbf{M} = \int_{\mathbb{R}} \phi_h(z) dz$ , see Fig. 7. This condition represents a mass constraint—the quasi-bilayer can be the dominant repository of mass only if the initial data has a compatible mass constitution. On the longer time-scale  $\tau_2 = \varepsilon^2 t$ , we show that any quasi-bilayer profile initial data evolves as a quasi-bilayer at leading order subject to a mass preserving Willmore flow that incorporates the intrinsic curvature of the associated quasi-bilayer  $\Phi_h$ , defined in (1.15).

In the outer region  $\Omega \setminus \Gamma_{l_0}$  we have the expansions,

$$\begin{cases} \mathbf{u}(x, \tau_\alpha; \varepsilon) = \mathbf{u}_0 + \varepsilon\mathbf{u}_1 + \varepsilon^2\mathbf{u}_2 + \varepsilon^3\mathbf{u}_3 + \mathcal{O}(\varepsilon^4), \\ \mu(x, \tau_\alpha; \varepsilon) = \mu_0 + \varepsilon\mu_1 + \varepsilon^2\mu_2 + \varepsilon^3\mu_3 + \mathcal{O}(\varepsilon^4). \end{cases}$$

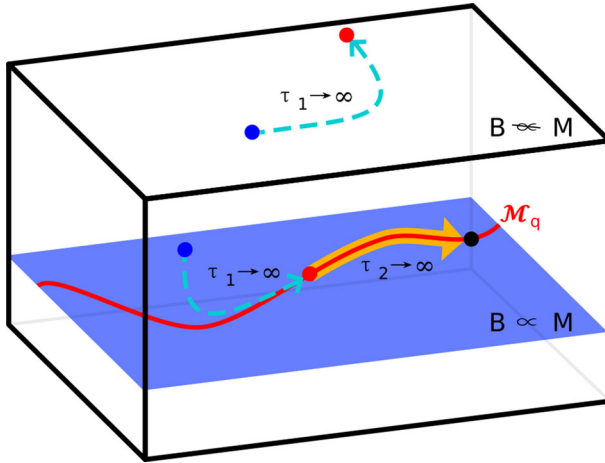


**Fig. 7** A reduced dimension “cartoon” depiction of the multi-time-scale geometric flow that drives pseudo-bilayers onto the affine subspace of quasi-bilayers. The *cuboid* represents the set of pseudo-bilayers, the *blue surface* represents the set of pseudo-bilayers with leading order background state  $\varepsilon\mathbf{B}$  proportional to the quasi-bilayer mass vector  $\mathbf{M}$  and the red curve represents the set of quasi-bilayers,  $\mathcal{M}_q$ . On the fast time scale,  $\tau = \varepsilon t$ , the *light-blue dashed curve* depicts the evolution of a typical pseudo-bilayer initial data with  $\mathbf{B} \propto \mathbf{M}$  (deep blue dot on the blue surface), which converges to its fast time equilibrium, (red dot); pseudo-bilayers with  $\varepsilon\mathbf{B}$  not proportional to  $\mathbf{M}$  cannot converge to slow time equilibrium not on  $\mathcal{M}_q$ . While  $\mathcal{M}_q$  is composed of fast-time equilibria, large transients occur within  $\mathcal{M}_q$  on the slow time scale  $\tau_2 = \varepsilon^2 t$ , governed by the mass preserving Willmore flow, (4.14), depicted by *thick orange curve* connecting the fast time equilibrium (red dot) to its slow time equilibrium (black dot) (colour figure online)

while in the inner region  $\Gamma_{l_0}$  the expansions take the form

$$\begin{cases} \mathbf{u}(x, \tau_\alpha; \varepsilon) = \tilde{\mathbf{u}}(z, s, \tau_\alpha; \varepsilon) = \tilde{\mathbf{u}}_0 + \varepsilon \tilde{\mathbf{u}}_1 + \varepsilon^2 \tilde{\mathbf{u}}_2 + \varepsilon^3 \tilde{\mathbf{u}}_3 + \mathcal{O}(\varepsilon^4), \\ \mu(x, \tau_\alpha; \varepsilon) = \tilde{\mu}(z, s, \tau_\alpha; \varepsilon) = \tilde{\mu}_0 + \varepsilon \tilde{\mu}_1 + \varepsilon^2 \tilde{\mu}_2 + \varepsilon^3 \tilde{\mu}_3 + \mathcal{O}(\varepsilon^4). \end{cases}$$

The time derivative involving the normal velocity of the interface admits the expansion,

$$\varepsilon^\alpha \mathbf{u}_{\tau_\alpha}(x, \tau_\alpha; \varepsilon) = \varepsilon^q [\partial_{\tau_\alpha} \tilde{\mathbf{u}} + \partial_s \tilde{\mathbf{u}} \partial_{\tau_\alpha} s + \partial_z \tilde{\mathbf{u}} \partial_{\tau_\alpha} r] = -\varepsilon^{q-1} V_{n,0} \partial_z \tilde{\mathbf{u}} + \mathcal{O}(\varepsilon^q),$$

where  $\mathbf{n} \cdot \partial_{\tau_\alpha} \Xi := V_n(s, \tau_\alpha; \varepsilon) = V_{n,0} + \varepsilon V_{n,1} + \mathcal{O}(\varepsilon^2)$ . More specifically, we have

$$\begin{cases} \mu_0 = \nabla_{\mathbf{u}}^2 W(\mathbf{u}_0) \nabla_{\mathbf{u}} W(\mathbf{u}_0), \\ \mu_1 = -\nabla_{\mathbf{u}}^2 W(\mathbf{u}_0) (-\nabla_{\mathbf{u}}^2 W(\mathbf{u}_0) \mathbf{u}_1 + \mathbf{V}(\mathbf{u}_0)) - [-\nabla_{\mathbf{u}}^3 W(\mathbf{u}_0) \mathbf{u}_1 + (\nabla_{\mathbf{u}} \mathbf{V}(\mathbf{u}_0))^T] \nabla_{\mathbf{u}} W(\mathbf{u}_0), \\ \mu_2 = -\nabla_{\mathbf{u}}^2 W(\mathbf{u}_0) [\Delta \mathbf{u}_0 - \nabla_{\mathbf{u}}^2 W(\mathbf{u}_0) \mathbf{u}_2 - \frac{1}{2} \nabla_{\mathbf{u}}^3 W(\mathbf{u}_0) (\mathbf{u}_1, \mathbf{u}_1) + \nabla_{\mathbf{u}} \mathbf{V}(\mathbf{u}_0) \mathbf{u}_1] \\ \quad + [-\nabla_{\mathbf{u}}^3 W(\mathbf{u}_0) \mathbf{u}_1 + (\nabla_{\mathbf{u}} \mathbf{V}(\mathbf{u}_0))^T] (-\nabla_{\mathbf{u}}^2 W(\mathbf{u}_0) \mathbf{u}_1 + \mathbf{V}(\mathbf{u}_0)) \\ \quad - [\Delta - \nabla_{\mathbf{u}}^3 W(\mathbf{u}_0) \mathbf{u}_2 - \frac{1}{2} \nabla_{\mathbf{u}}^4 W(\mathbf{u}_0) (\mathbf{u}_1, \mathbf{u}_1) + (\nabla_{\mathbf{u}}^2 \mathbf{V}(\mathbf{u}_0) \mathbf{u}_1)^T] \nabla_{\mathbf{u}} W(\mathbf{u}_0) - \eta_2 \nabla_{\mathbf{u}} W(\mathbf{u}_0), \end{cases}$$

and

$$\begin{cases} \tilde{\mu}_0 = \mathbf{I}_0 \mathbf{\Pi}_0, \\ \tilde{\mu}_1 = \mathbf{I}_0 \mathbf{\Pi}_1 + \mathbf{I}_1 \mathbf{\Pi}_0, \\ \tilde{\mu}_2 = \mathbf{I}_0 \mathbf{\Pi}_2 + \mathbf{I}_1 \mathbf{\Pi}_1 + \mathbf{I}_2 \mathbf{\Pi}_0 + \mathbf{\Pi} \mathbf{\Pi}_2, \\ \tilde{\mu}_3 = \mathbf{I}_0 \mathbf{\Pi}_3 + \mathbf{I}_1 \mathbf{\Pi}_2 + \mathbf{I}_2 \mathbf{\Pi}_1 + \mathbf{I}_3 \mathbf{\Pi}_0 + \mathbf{\Pi} \mathbf{\Pi}_3, \end{cases}$$

where

$$\begin{cases} \partial_z^2 + \varepsilon H(z, s) \partial_z + \varepsilon^2 \Delta_G - \nabla_{\mathbf{u}}^2 W(\tilde{\mathbf{u}}) + \varepsilon (\nabla_{\mathbf{u}} \mathbf{V}(\tilde{\mathbf{u}}))^T := \mathbf{I} = \mathbf{I}_0 + \varepsilon \mathbf{I}_1 + \dots, \\ (\partial_z^2 + \varepsilon H(z, s) \partial_z + \varepsilon^2 \Delta_G) \tilde{\mathbf{u}} - \nabla_{\mathbf{u}} W(\tilde{\mathbf{u}}) + \varepsilon \mathbf{V}(\tilde{\mathbf{u}}) := \mathbf{\Pi} = \mathbf{\Pi}_0 + \varepsilon \mathbf{\Pi}_1 + \dots, \\ -\varepsilon^2 [-\eta_1 (\partial_z^2 + \varepsilon H(z, s) \partial_z + \varepsilon^2 \Delta_G) \tilde{\mathbf{u}} + \eta_2 \nabla_{\mathbf{u}} W(\tilde{\mathbf{u}})] := \mathbf{\Pi} \mathbf{\Pi} = \mathbf{\Pi} \mathbf{\Pi}_0 + \varepsilon \mathbf{\Pi} \mathbf{\Pi}_1 + \dots, \end{cases}$$

We follow the usual matching procedure, first employed for the Cahn–Hilliard equation in [Pego \(1989\)](#), for the inner and outer expansions; that is, for any given  $x \in \Gamma$ , we require that

$$\begin{aligned} &(\mathbf{u}_0 + \varepsilon \mathbf{u}_1 + \varepsilon^2 \mathbf{u}_2 + \varepsilon^3 \mathbf{u}_3 + \dots)(x + \varepsilon z \mathbf{n}, \tau_\alpha) \\ &\approx (\tilde{\mathbf{u}}_0 + \varepsilon \tilde{\mathbf{u}}_1 + \varepsilon^2 \tilde{\mathbf{u}}_2 + \varepsilon^3 \tilde{\mathbf{u}}_3 + \dots)(z, s, \tau_\alpha). \end{aligned}$$

For the cases  $\alpha = -2, -1, 0, 1$ , the calculation closely follows the scalar case presented in [Dai and Promislow \(2013\)](#), and shows that any quasi-bilayer profile is an equilibrium of the corresponding leading-order evolution system. We provide details for the slow time scale  $\tau_1 = \varepsilon t$  with initial pseudo-bilayer profile and the slow time scale  $\tau_2 = \varepsilon^2 t$  with initial data a quasi-bilayer profile obtained as equilibrium of the  $\tau_1$  evolution.

*Time scale  $\tau_1 = \varepsilon t$ : a quenched mean curvature flow.* We study the initial-value problem,

$$\begin{cases} \varepsilon \mathbf{u}_{\tau_1}(x, \tau_1) = \Delta \mu(x, \tau_1), \\ \mathbf{u}(x, 0) = \mathbf{u}_p(x, \varepsilon; \mathbf{B}_0, \Gamma_0). \end{cases} \tag{4.3}$$

At leading order the outer expansion takes the form,

$$\begin{cases} \mu_0 = 0, \\ \mu_1 = (\nabla_{\mathbf{u}}^2 W(0))^2 \mathbf{u}_1, \quad \Delta \mu_1 = 0. \end{cases} \tag{4.4}$$

while the leading order terms in the inner expansion take the form,

$$\begin{cases} \tilde{\mu}_0 = 0, \\ \partial_z^2 \tilde{\mu}_1 = 0, \\ -V_{n,0} \partial_z \phi_h = H_0(s) \partial_z \tilde{\mathbf{u}}_1 + \partial_z^2 \tilde{\mathbf{u}}_2. \end{cases} \tag{4.5}$$

A analysis similar to that in Dai and Promislow (2013) yields the following leading-order evolution system, for  $\tau_1 \geq 0$ ,

$$\begin{cases} \tilde{\mathbf{u}}_0 = \phi_h(z), & \mathbf{u}_0 = 0, & (4.6a) \\ \mu_1 = \tilde{\mu}_1 = \mathbf{B}_1(\tau_1), & & (4.6b) \\ \tilde{\mathbf{u}}_1 = (\mathcal{L}_{0,\perp})^{-2}(\mathbf{B}_1(\tau_1) - \mathcal{L}_0\mathbf{V}(\phi_h)), & & (4.6c) \\ \mathbf{u}_1 = \left(\nabla_{\mathbf{u}}^2 W(0)\right)^{-2} \mathbf{B}_1(\tau_1), & & (4.6d) \\ V_{n,0} = \frac{\mathbf{B}_1(\tau_1) \cdot \mathbf{M}}{M_2} H_0, & & (4.6e) \end{cases}$$

where  $\mathbf{B}_1(0) = (\nabla_{\mathbf{u}} W(0))^2 \mathbf{B}_0$  and we recall that  $\mathbf{M} = \int_{\mathbb{R}} \phi_h(z) dz$  and  $M_2 = \int_{\mathbb{R}} |\phi_h(z)|^2 dz$ . From (4.6b–4.6d), we have

$$\mathbf{u}(x, \tau_1; \varepsilon) = \begin{cases} \phi_h(z(x)) + \varepsilon \tilde{\mathbf{u}}_1(x, \tau_1) + \mathcal{O}(\varepsilon^2), & x \in \Gamma_{l_0}, \\ \varepsilon (\nabla_{\mathbf{u}}^2 W(0))^{-2} \mathbf{B}_1(\tau_1) + \mathcal{O}(\varepsilon^2), & x \in \Omega \setminus \Gamma_{l_0}, \end{cases}$$

whose  $\varepsilon$ -scaled mass vector  $\mathcal{M}$ , defined in (1.9), admits the expansion,

$$\mathcal{M}(\tau_1) = |\Omega| (\nabla_{\mathbf{u}}^2 W(0))^{-2} \mathbf{B}_1(\tau_1) + |\Gamma|(\tau_1) \mathbf{M} + \mathcal{O}(\varepsilon).$$

Expanding the mass vector  $\mathcal{M} = \mathcal{M}_1 + \mathcal{O}(\varepsilon)$  and the interface area  $|\Gamma|(\tau_1) = \gamma_0(\tau_1) + \mathcal{O}(\varepsilon)$ , we have

$$\mathcal{M}_1 = |\Omega| (\nabla_{\mathbf{u}}^2 W(0))^{-2} \mathbf{B}_1(\tau_1) + \gamma_0(\tau_1) \mathbf{M}. \tag{4.7}$$

Under a prescribed normal velocity, the time derivative of the surface area equals the integral of the product of mean curvature and normal velocity over the surface, that is,

$$\partial_{\tau_1} |\Gamma| = \int_S H_0 V_n dS, \tag{4.8}$$

where  $\mathbf{r}(s) : S \rightarrow \Gamma$  is the parameterization of the interface  $\Gamma$ . At leading order, (4.8) takes the form  $\partial_{\tau_1} \gamma_0 = M_2^{-1} (\mathbf{B}_1(\tau_1) \cdot \mathbf{M}) \int_S H_0^2 dS$ . Defining the quantity

$$E(\tau_1) := \mathbf{B}_1(\tau_1) \cdot \mathbf{M},$$

then (4.8) and (4.7) prescribe the evolution of  $E$ , that is,

$$\partial_{\tau_1} E = - \frac{\mathbf{M}^T [\nabla_{\mathbf{u}}^2 W(0)]^2 \mathbf{M}}{|\Omega| M_2} E \int_S H_0^2 dS. \tag{4.9}$$

It is straightforward to deduce the following lemma from (4.6, 4.7, 4.9).

**Lemma 4.1** *Given a pseudo-bilayer  $\mathbf{u}_p(x, \varepsilon; \mathbf{B}_0, \Gamma_0)$  with the mean curvature of the initial interface  $\Gamma_0$  far away from zero, the evolution of the pseudo-bilayer in the time scale  $\tau_1 = \varepsilon t$  satisfies the leading-order evolution system (4.6) with*

$$\lim_{\tau_1 \rightarrow \infty} \mathbf{B}_1(\tau_1) \cdot \mathbf{M} = 0, \quad \lim_{\tau_1 \rightarrow \infty} V_{n,0} = 0,$$

where  $\lim_{\tau_1 \rightarrow \infty} \mathbf{B}_1(\tau_1) = 0$  if and only if the leading order term of the mass vector  $\mathcal{M}_1$ , defined in rm (1.9), is proportional to  $\mathbf{M}$ . Moreover, any quasi-bilayer profile  $\mathbf{u}_q$  associated to  $\{\mathbf{m}_0, \Gamma_0\}$  is an equilibrium of the leading-order evolution system (4.6) on time scales up to  $\tau_1$ .

*Remark 4.2* The convergence of the quantity  $E(\tau_1) := \mathbf{B}_1(\tau_1) \cdot \mathbf{M}$  towards zero has a straightforward physical interpretation: for the single-component case, the growing length of the bilayer depletes the amphiphiles in the far-field, or background, region. The multicomponent bilayer reaches its maximal length when the inner product of the bilayer mass vector,  $\mathbf{M}$ , with the far field amphiphile density  $\mathbf{B}$  is zero. However it requires tuning of the initial mass fractions to have all species reach zero in the far-field simultaneously. That is, while  $\lim_{\tau_1 \rightarrow \infty} \mathbf{B}_1(\tau_1) \cdot \mathbf{M} = 0$ , it is non-generic that this coincides with the ‘emptying’ of the far-field region, so that generically  $\lim_{\tau_1 \rightarrow \infty} \mathbf{B}_1(\tau_1) \neq 0$ . For a two species blend, that is  $N = 2$ , the existence of a one-parameter family of homoclinics, as in the universal Birkhoff-billard Example 3.4, would remove this condition as the bilayer composition could adapt continuously to the the available amphiphile supply.

*Time scale  $\tau_2 = \varepsilon^2 t$ : surface-area-preserving Willmore flow* We study the evolution of the set of quasi-bilayers  $\mathcal{M}_q$  in the slow time scale  $\tau_2 = \varepsilon^2 t$ , assuming that the  $O(\varepsilon)$  components of the background profile  $\mathbf{B}$  has converged to zero on the fast,  $\tau_1$ , time scale. For the slow,  $\tau_2$  time-scale, the initial profile is a quasi-bilayer  $\mathbf{u}_q$  associated with interface  $\{\mathbf{m}_0, \Gamma_0\}$ . This corresponds to the inner and outer expansions

$$\tilde{\mathbf{u}}_0(z, s, 0) = \phi_h(z), \quad \tilde{\mathbf{u}}_1(z, s, 0) = \phi_{h,1}(z), \quad \mathbf{u}_0(x, 0) = \mathbf{u}_1(x, 0) = 0. \quad (4.10)$$

A straightforward but lengthy calculation shows that at the leading-order the solution  $u$  of the initial value problem (4.1) remains a quasi-bilayer, parameterized by its  $O(\varepsilon^2)$  back-ground state  $\mathbf{B}_2$  and the interface  $\Gamma$ , whose evolution is given by, for  $\tau_2 \geq 0$ ,

$$\left\{ \begin{array}{l} \tilde{\mathbf{u}}_0(z, s, \tau_2) \equiv \phi_h(z), \quad \tilde{\mathbf{u}}_1(z, s, \tau_2) \equiv \phi_{h,1}(z), \quad \mathbf{u}_0(x, \tau_2) = \mathbf{u}_1(x, \tau_2) \equiv 0, \end{array} \right. \quad (4.11a)$$

$$\left\{ \begin{array}{l} \mu_2(x, \tau_2) = \tilde{\mu}_2(x, \tau_2) = \mathbf{B}_2(\tau_2), \end{array} \right. \quad (4.11b)$$

$$\left\{ \begin{array}{l} V_{n,0}(s, \tau_2) = \frac{M_1}{M_2} \left[ \Delta_s H_0 + \left( \frac{\eta_1 + \eta_2}{2} + \frac{\mathbf{B}_2 \cdot \mathbf{M}}{M_1} \right) H_0 - \frac{1}{2} H_0 (H_0 - a_0)^2 - H_1 (H_0 - a_0) \right], \end{array} \right. \quad (4.11c)$$



where we recall  $M_1 := \int_{\mathbb{R}} |\partial_z \phi_h|^2 dz$ . We calculate the  $\varepsilon$ -scaled total mass vector  $\mathcal{M}$  of the amphiphiles, that is,

$$\mathcal{M} = |\Gamma| \mathbf{M} + \varepsilon \left[ |\Omega| (\nabla_{\mathbf{u}}^2 W(0))^{-2} \mathbf{B}_2 + |\Gamma| \int_{\mathbb{R}} \phi_{h,1} dz + \int_S H_0(s) dS \int_{\mathbb{R}} z \phi_h(z) dz \right] + \mathcal{O}(\varepsilon^2).$$

Given the area expansion  $|\Gamma|(\tau_2) = \gamma_0(\tau_2) + \mathcal{O}(\varepsilon)$  and the mass expansion  $\mathcal{M} = M_1 + \mathcal{O}(\varepsilon)$ , it is straightforward to see that

$$\gamma_0(\tau_2) \equiv |\Gamma_0|. \tag{4.12}$$

Moreover, plugging the expression of  $V_{n,0}$  (4.11c) into the surface area evolution equation (4.8), yields the evolution of the background state

$$\mathbf{B}_2 \cdot \mathbf{M} = -M_1 \frac{\int_S [ -|\nabla_s H_0|^2 + \frac{\eta_1 + \eta_2}{2} H_0^2 - \frac{1}{2} H_0^2 (H_0 - a_0)^2 - H_1 H_0 (H_0 - a_0) ] dS}{\int_S H_0^2 dS}.$$

Introducing the zero-mass projection operator

$$\Pi_{\Gamma}(f) = f - H_0 \frac{\int_S f H_0 dS}{\int_S H_0^2 dS}, \tag{4.13}$$

We conclude that, under the mass conservation, the normal velocity of the interface takes the form

$$V_{n,0} = \frac{M_1}{M_2} \Pi_{\Gamma} \left[ \left( \Delta_s - \frac{1}{2} H_0 (H_0 - a_0) - H_1 \right) (H_0 - a_0) \right], \tag{4.14}$$

which, together with the area preserving equation (4.12), completes the derivation of Formal Result 1.

### 4.1 Evolution of radial bilayers under the mass preserving Willmore flow

To demonstrate the dynamics of the area-preserving Willmore flow, (4.14), we consider the evolution of  $m$  well-separated spherically symmetric vesicle cells with radii  $\{R_i(\tau_2)\}_{i=1}^m$  in the domain  $\Omega \in \mathbb{R}^d$ . For the  $i$ -th sphere we have

$$H_0 = (d - 1)R_i^{-1}, \quad H_1 = -(d - 1)R_i^{-2},$$

and the normal velocity equation (4.14) reduces to

$$\frac{dR_i}{d\tau_2} = \frac{(d - 1)M_1}{2M_2} R_i^{-1} \left\{ [(3 - d)R_i^{-1} + a_0][(d - 1)R_i^{-1} - a_0] - R_c^{-2} \right\}, \tag{4.15}$$

where

$$R_c^{-2} := \frac{\sum_{j=1}^m [(3-d)R_j^{-1} + a_0][(d-1)R_j^{-1} - a_0]R_j^{d-3}}{\sum_{j=1}^m R_j^{d-3}}.$$

Conservation of the total interface area gives a first integral of the ODE system (4.15), that is,

$$\sum_{j=1}^m R_j^{d-1}(\tau_2) = m\bar{R}^{d-1},$$

where

$$\bar{R} := \sqrt[d-1]{\frac{1}{m} \sum_{j=1}^m R_j^{d-1}(0)}.$$

Consequently the only equilibrium of the system (4.15) is the equi-radius solution  $R_i = \bar{R}$  for all  $i = 1, 2, \dots, m$ . Linearizing the vector field of the ODE system about the equi-radius equilibrium we obtain the linearized matrix  $\mathbf{L}$  in the form,

$$\mathbf{L} = -\frac{(d-1)M_1}{M_2R^3} \left[ \frac{(d-1)(3-d)}{R} + (d-2)a_0 \right] \left( \mathbf{I}_m - \frac{1}{m}\mathbf{J}_m \right),$$

where  $\mathbf{J}_m$  denotes the  $m \times m$  matrix of all ones. The equi-radius equilibrium is stable for initial data for which

$$K(R, a_0, d) := \frac{(d-1)(3-d)}{\bar{R}} + (d-2)a_0 > 0, \tag{4.16}$$

and unstable when  $K < 0$ .

In space dimension  $d = 2$ , the intrinsic curvature term  $a_0$  drops out of the evolution of (4.15), which reduces to

$$\frac{dR_i}{d\tau_2} = \frac{M_1}{2M_2} R_i^{-1} \left( R_i^{-2} - \frac{\sum_{j=1}^m R_j^{-3}}{\sum_{j=1}^m R_j^{-1}} \right),$$

and admits a globally attracting equi-radius equilibrium  $R_i = \bar{R}$ , that is,

$$\lim_{\tau_2 \rightarrow \infty} R_i(\tau) = \bar{R}, \quad i = 1, 2, \dots, m.$$

For  $d > 2$ , the stability of the equi-radius equilibrium depends upon the value of the intrinsic curvature  $a_0$ . More specifically, for  $d = 3$ , we have

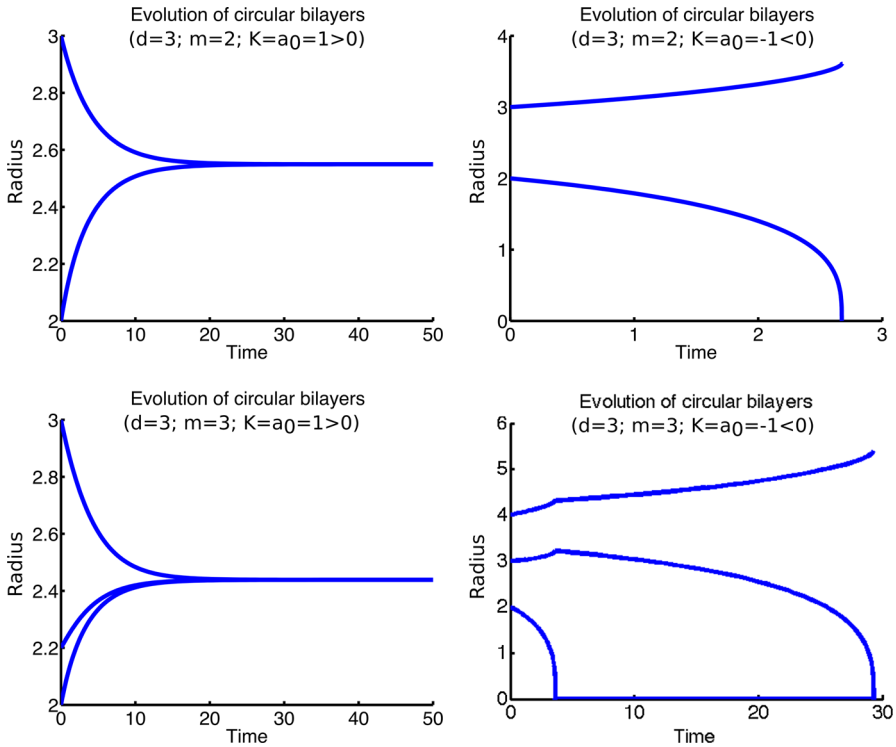


**Fig. 8** Simulation of the radius of  $m$  spheres with respect to time in spatial dimension  $d = 3$ . For  $a_0 > 0$  the equi-radius solution is asymptotically stable, while for  $a_0 < 0$  the smallest radius liposome extinguishes in finite time, leading to an eventual winner-take-all scenario

$$\frac{dR_i}{d\tau_2} = 2a_0 \frac{M_1}{M_2} R_i^{-1} \left( R_i^{-1} - \frac{1}{m} \sum_{j=1}^m R_j^{-1} \right),$$

where the stability of the equi-radius equilibrium depends uniquely upon the sign of  $a_0$ . In particular we find

$$\lim_{\tau \rightarrow \infty} R_i(\tau_2) = \begin{cases} \bar{R}, & a_0 > 0, \\ R_i(0), & a_0 = 0, \end{cases}$$

while for  $a_0 < 0$ , the equi-radius equilibrium is unstable. Figure 8 includes a simulation of the case  $a_0 < 0$  and  $m = 2$  and  $m = 3$  in which the smallest circular bilayer shrinks and disappears in finite time, leading to a coarsening phenomenon and eventually a winner-take-all scenario.

### 5 Conclusion

The multi-component functionalized Cahn–Hilliard (mFCH) free energy is a continuous model for multi-component amphiphilic blends, including plasma membranes, and its gradient flow describes their slow evolution. We established the existence of quasi-bilayers, a class of co-dimensional one morphologies which encompasses the orbits traced by the slow dynamics of bilayer dressings of admissible co-dimension one interfaces, and contains the associated stationary bilayer solutions. We showed that when evaluated on the set of quasi-bilayers, mFCH free energy reduces at leading order to the well-known Canham–Helfrich sharp interface free energy, with intrinsic curvature determined via a Melnikov parameter arising from the  $\varepsilon$ -order solenoidal perturbation  $\mathbf{V}$  of the mixing potential  $\mathbf{W}$ , (6.2). For the special class of regularized Birkhoff-billiard mixing potentials, we established the existence of  $n$ -striation quasi-bilayers for sufficiently small regularization parameter  $\delta \ll 1$ , and analyzed their layer-by-layer pearling bifurcation, showing that all order  $\mathcal{O}(\delta^{-2})$  eigenvalues are in one-to-one affiliation with a layer-collision and that the associated eigenmodes are localized near the collision point. This analysis establishes the layer-by-layer pearling observed experimentally. Finally we used formal multi-scale asymptotics to derive the evolution of quasi-bilayers under the  $H^{-1}$  gradient flow of the mFCH, establishing that on the slow time scale  $\tau_2 = \varepsilon^2 t$ , the evolution of admissible interfaces follows a mass-preserving Willmore flow. Moreover for radially symmetric bilayers, the intrinsic curvature selects between regimes in which the bilayers seek a common equilibrium radius and a winner-take-all regime in which the smallest radius bilayer is extinguished in finite time.

Beyond bilayer morphologies, the mFCH free energy accommodates a cornucopia of higher codimensional network structures whose interactions and rich dynamics are unexplored; moreover the possible complexity of purely bilayer evolution is only hinted at in this work. Indeed, of particular interest are Birkhoff-billiard potentials which admit a family of homoclinics parametrized by one or more independent parameters, such as the universal billiard potential given in Example 3.4; the associated linearization, (3.3) of the underlying dynamical system has a non-trivial kernel, and the associated slow dynamics will couple the geometric evolution arising from the translational eigenmode to the compositional evolution associated to the hidden symmetries. Taking the functionalization parameter  $\eta_1$  and  $\eta_2$  to depend on  $\mathbf{u}$  encodes amphiphile preference for curvature and co-dimension, and yields a dynamic competition in which bilayer composition interacts with the geometric evolution and could for example trigger bifurcations leading to endocytosis.

In biological settings, plasma membranes are generically very stable, in particular they are not generically susceptible to pearling bifurcations. This strict stability to pearling is also generic within the mFCH: indeed the term  $\mathbf{G}_1$  in (6.1), is not typically the gradient of a scalar function, and one anticipates a more genetical form for the mFCH,

$$\mathcal{F}_{gM}(\mathbf{u}) = \int_{\Omega} \frac{1}{2} |\varepsilon^2 \mathbf{D}\Delta \mathbf{u} - \mathbf{G}(\mathbf{u})|^2 - \varepsilon^2 P(\mathbf{u}) dx, \tag{5.1}$$

where  $\nabla \times \mathbf{G} \neq 0$ . Assuming the existence of an orbit  $\phi_h$  of

$$\mathbf{D}\partial_z^2 \mathbf{u} - \mathbf{G}(\mathbf{u}) = 0,$$

which is homoclinic to zero, the associated linearization  $\mathcal{L}_g := \mathbf{D}\partial_z^2 - \nabla_{\mathbf{u}}\mathbf{G}(\phi_h)$  is generically not self-adjoint. The second functional derivative of  $\mathcal{F}_{gM}(\mathbf{u}_h)$ , evaluated at a dressing,  $\mathbf{u}_h$ , of an admissible interface with the homoclinic  $\phi_h$ , admits the expansion,

$$\mathbb{L}_g := \frac{\delta^2 \mathcal{F}_{gM}}{\delta \mathbf{u}^2}(\mathbf{u}_h) = (\mathcal{L}_g^T + \varepsilon \Delta_s)(\mathcal{L}_g + \varepsilon \Delta_s) + \mathcal{O}(\varepsilon).$$

In many situations (Doelman et al. 1998, 2001, 2002) the spectra of  $\mathcal{L}_g$  is comprised of eigenvalues  $\{\lambda_k\}_{k=1}^N$  with positive real part but with nonzero, order  $\mathcal{O}(1)$  imaginary part. The corresponding pearling eigenvalues of  $\mathbb{L}_g$  take the form  $\Lambda_{k,n} = |\lambda_k - \varepsilon^2 \beta_n|^2 + \mathcal{O}(\varepsilon)$ , where the real Laplace–Beltrami eigenvalues  $\beta_n > 0$  are always an  $\mathcal{O}(1)$  distance away from the strictly complex  $\lambda_k$ . The lack of positive, purely-real eigenvalues of  $\mathcal{L}_g$  robustly inhibits pearling and suggests the provocative statement: the choices available in the packing of lipids within multicomponent membranes generically serves to inhibit the mechanisms of pearling. This simple analysis is in sympathy with diverse observations of plasma membranes; and suggests that dynamical systems has a potentially significant role to play in our understanding of the nature of these essential components of cellular design.

**Acknowledgements** The first author acknowledges supported by the National Science Foundation through Grant DMS-1409940. Both authors thank Brian Wetton for providing numerical simulations in support of the analysis and Arjen Doelman for several beneficial discussions.

## 6 Appendix: The multicomponent Gommper–Schick free energy and its mFCH reduction

We introduce the multicomponent Gommper–Schick (mGS) free energy and obtain the mFCH as a reduction. The scalar Gommper Shick free energy (Gompper and Schick 1990), takes the form (1.1),

$$\mathcal{F}_{GS}(u) = \int_{\Omega} \varepsilon^4 \frac{1}{2} |\Delta u|^2 + \varepsilon^2 G_1(u) \Delta u + G_2(u) dx,$$

which we generalize for the vector case to the mGS free energy

$$\mathcal{F}_{mGS}(\mathbf{u}) = \int_{\Omega} \frac{\varepsilon^4}{2} |\mathbf{D}\Delta \mathbf{u}|^2 + \varepsilon^2 \mathbf{G}_1(\mathbf{u}) \cdot \mathbf{D}\Delta \mathbf{u} + G_2(\mathbf{u}) dx, \tag{6.1}$$

where the matrix,  $\mathbf{D} = \text{diag}(d_1, d_2, \dots, d_N) > 0$ , encodes the differences in molecular length and weight between the amphiphilic species. A key step in the selection of a minimal reduction of the mGS that preserves the richness of its solution space is the observation that for  $N > 1$  vector valued functions  $\mathbf{G} : \mathbb{R}^N \mapsto \mathbb{R}^N$  are not

generically gradients of a scalar valued function. In the spirit of a minimal model, we take

$$\mathbf{G}_1(\mathbf{u}) := -\nabla_{\mathbf{u}}W(\mathbf{u}) + \varepsilon\mathbf{V}(\mathbf{u}), \tag{6.2}$$

for which the generic *solenoidal* perturbation  $\mathbf{V} : \mathbb{R}^N \mapsto \mathbb{R}^N$  satisfies  $\nabla_{\mathbf{u}} \times \mathbf{V} \neq 0$ , in contrast to the irrotational term  $\nabla_{\mathbf{u}}W$  whose curl is zero. The most restrictive assumption on the form of the mGS, which parallels that made for the scalar case, is that the energy is close to a perfect square, specifically, within the context of the weak functionalization,  $G_2$  takes the form

$$G_2(\mathbf{u}) := \frac{1}{2} |-\nabla_{\mathbf{u}}W(\mathbf{u}) + \varepsilon\mathbf{V}(\mathbf{u})|^2 - \varepsilon^2 P(\mathbf{u}),$$

where the perturbation  $P : \mathbb{R}^N \mapsto \mathbb{R}$  is smooth. Within this framework, the multi-component functionalized Cahn–Hilliard (mFCH) free energy takes the form

$$\mathcal{F}_M(\mathbf{u}) = \int_{\Omega} \frac{1}{2} |\varepsilon^2 \mathbf{D}\Delta\mathbf{u} - \nabla_{\mathbf{u}}W(\mathbf{u}) + \varepsilon\mathbf{V}(\mathbf{u})|^2 - \varepsilon^2 P(\mathbf{u}) dx. \tag{6.3}$$

To separate out the amphiphilicity term within the functionalization we make one last adjustment, redefining  $W = \tilde{W}(\mathbf{u}) - \varepsilon^2 Q(\mathbf{D}^{-\frac{1}{2}}\mathbf{u})$ , so that  $\nabla_{\mathbf{u}}W = \nabla_{\mathbf{u}}\tilde{W} - \varepsilon^2 \mathbf{D}^{-\frac{1}{2}}\nabla_{\mathbf{u}}Q$ , we may re-expand the quadratic term, which yields

$$\begin{aligned} \mathcal{F}_M(\mathbf{u}) &= \int_{\Omega} \frac{1}{2} |\varepsilon^2 \mathbf{D}\Delta\mathbf{u} - \nabla_{\mathbf{u}}\tilde{W}(\mathbf{u}) + \varepsilon\mathbf{V}(\mathbf{u})|^2 \\ &\quad - \varepsilon^2 \left( \tilde{P}(\mathbf{u}) - \varepsilon^2 \mathbf{D}^{\frac{1}{2}}\Delta\mathbf{u} \cdot \nabla_{\mathbf{u}}Q(\mathbf{D}^{-\frac{1}{2}}\mathbf{u}) \right) dx, \end{aligned}$$

where  $\tilde{P} = P + \nabla_{\mathbf{u}}\tilde{W} \cdot \mathbf{D}^{-\frac{1}{2}}\nabla_{\mathbf{u}}Q + \mathcal{O}(\varepsilon)$ . Dropping the tilde notation, integration by parts on the last term yields the form

$$\begin{aligned} \mathcal{F}_M(\mathbf{u}) &= \int_{\Omega} \frac{1}{2} |\varepsilon^2 \mathbf{D}\Delta\mathbf{u} - \nabla_{\mathbf{u}}W(\mathbf{u}) + \varepsilon\mathbf{V}(\mathbf{u})|^2 \\ &\quad - \varepsilon^2 \left( P(\mathbf{u}) + \varepsilon^2 \nabla_{\mathbf{u}} : \mathbf{D}^{\frac{1}{2}}\nabla_{\mathbf{u}}^2 Q \mathbf{D}^{-\frac{1}{2}}\nabla_{\mathbf{u}} \right) dx, \end{aligned} \tag{6.4}$$

where the symbol  $:$  denotes the double-contraction inner product that generates the usual norm on  $\mathbb{R}^{N \times d}$ . In their density functional based model, [Andreussi et al. \(2012\)](#) found that effective parameterization of solvation energies of solutes required two fit parameters associated to the quantum surface area and quantum volume associated to solvent-excluded region about the solute. In this spirit, we reduce the functionalization terms within the mFCH to an equivalent two-parameter family. Generically we assume that  $Q$  is positive definite, so that its Hessian is a positive definite matrix, however for the two-parameter reduction we further restrict  $Q$  to take the form

$$Q(\mathbf{D}^{-\frac{1}{2}}\mathbf{u}) = \frac{1}{2} \eta_1 |\mathbf{u}|^2,$$

where the parameter  $\eta_1 > 0$  encodes the (common) strength of the hydrophilic interaction of the amphiphilic species with the solvent.

To better motivate a simplified form for  $P$ , we note that the co-dimension one bilayer morphologies are described to leading order by solutions,  $\phi_h$  of the second order system

$$\partial_z^2 \mathbf{u} = \nabla_{\mathbf{u}} W(\mathbf{u}), \tag{6.5}$$

where  $z$  is signed, scaled distance normal to the bilayer, and  $u$  is homoclinic to the solvent phase  $\mathbf{u} = 0$ . The impact of  $P$  is perturbative; for a quasi-critical point  $\mathbf{u}_c$  of associated Cahn–Hilliard free energy, that is a solution of (1.3), the residual of the dominant quadratic term in (6.4) arises at the same asymptotic order as the functionalization terms. The volume integral of the functionalized term,  $\varepsilon^2 \int_{\Omega} P(\mathbf{u}_c) dx$ , contributes at the same order as the Helfrich term in the quadratic residual, balancing packing entropy against geometry. The Hamiltonian structure of (6.5) requires that solutions homoclinic to zero reside on the set  $\{\mathbf{u} \mid W(\mathbf{u}) \geq 0\}$  while higher co-dimensional profiles enter the region  $\{\mathbf{u} \mid W(\mathbf{u}) < 0\}$ . This observation motivates the choice of  $P$  as a scalar multiple of  $W$ , since volume integrals of  $W(\mathbf{u})$  make a positive contribution for bilayers, but give zero or negative contributions for codimension two and three morphologies.

**Assumption 6.1** We consider the mFCH, (6.4), with the simplified form for the functionalization terms

$$\mathbf{D} = \mathbf{I}_N, \quad Q(\mathbf{D}^{-\frac{1}{2}} \mathbf{u}) = \frac{1}{2} \eta_1 |\mathbf{u}|^2, \quad \mathbf{P}(\mathbf{u}) = \eta_2 W(\mathbf{u}), \quad \mathbf{V}(0) = 0, \quad W(0) = 0,$$

where  $\eta_1 \in \mathbb{R}^+$ ,  $\eta_2 \in \mathbb{R}$  are parameters. Moreover, the origin is a strict local minima of the mixing potential  $W$ , with a strictly positive-definite Hessian:  $\nabla_u^2 W(0) > 0$ .

Under Assumption 6.1, the multi-component weak FCH free energy takes the final form as in (1.6)

$$\mathcal{F}_M(\mathbf{u}) = \int_{\Omega} \frac{1}{2} |\varepsilon^2 \Delta \mathbf{u} - \nabla_{\mathbf{u}} W(\mathbf{u}) + \varepsilon \mathbf{V}(\mathbf{u})|^2 - \varepsilon^2 \left( \varepsilon^2 \frac{\eta_1}{2} |\nabla \mathbf{u}|^2 + \eta_2 W(\mathbf{u}) \right) dx.$$

## References

Alexandridis P, Lindman B (2000) Amphiphilic block copolymers: self-assembly and applications. Elsevier, Amsterdam

Ameduri B (2009) From vinylidene fluoride (VDF) to the applications of VDF-containing polymers and copolymers: recent developments and future trends. Chem Rev 109:6632–6686

Andreussi O, Dabo I, Marzari N (2012) Revised self-consistent continuum solvation in electronic-structure calculations. J Chem Phys 136. doi:10.1063/1.3676407

Birkhoff G, Rota G-C (1989) Ordinary differential equations, 4th edn. Wiley, New York

Budin I, Szostak J (2011) Physical effects underlying the transition from primitive to modern cell membranes. Proc Natl Acad Sci 108:5249–5254

Canham P (1970) The minimum energy of bending as a possible explanation of the biconcave shape of the human red blood cell. J Theor Biol 26:61–81

Cohen F, Melikyan G (2004) The energetics of membrane fusion from binding, through hemifusion, pore formation, and pore enlargement. J Membr Biol 199:1–14

- Dai S, Promislow K (2013) Geometric evolution of bilayers under the functionalized Cahn–Hilliard equation. *Proc R Soc A Math Phys Eng Sci* 469. doi:[10.1098/rspa.2012.0505](https://doi.org/10.1098/rspa.2012.0505)
- Doelman A, Gardner RA, Kaper TJ (1998) Stability analysis of singular patterns in the 1D Gray–Scott model: a matched asymptotics approach. *Phys D* 122:1–36
- Doelman A, Gardner RA, Kaper TJ (2001) Large stable pulse solutions in reaction-diffusion equations. *Indiana Univ Math J* 50:443–507
- Doelman A, Gardner RA, Kaper TJ (2002) A stability index analysis of 1-D patterns of the Gray–Scott model. *Membr Am Math Soc* 155:xii+64
- Doelman A, Hayrapetyan G, Promislow K, Wetton B (2014) Meander and pearling of single-curvature bilayer interfaces in the functionalized Cahn–Hilliard equation. *SIAM J Math Anal* 46:3640–3677
- Gavish N, Hayrapetyan G, Promislow K, Yang L (2011) Curvature driven flow of bi-layer interfaces. *Phys D Nonlinear Phenom* 240:675–693
- Gompper G, Schick M (1990) Correlation between structural and interfacial properties of amphiphilic systems. *Phys Rev Lett* 65:1116–1119
- Hanton SL, Bortolotti LE, Renna L, Stefano G, Brandizzi F (2005) Crossing the divide-transport between the endoplasmic reticulum and golgi apparatus in plants. *Traffic* 6:267–277
- Hayrapetyan G, Promislow K (2014) Spectra of functionalized operators arising from hypersurfaces. *Zeitschrift für angewandte Mathematik und Physik* 66:631–632
- Homburg AJ, Sandstede B (2010) Homoclinic and heteroclinic bifurcations in vector fields, *Handbook of dynamical systems III*. Elsevier, Amsterdam
- Jain S, Bates F (2004) Consequences of nonergodicity in aqueous binary PEO-PB micellar dispersions. *Macromolecules* 37:1511–1523
- Kapitula T, Promislow K (2013) Spectral and dynamical stability of nonlinear waves, vol. 185 of applied mathematical sciences. Springer, New York
- Kato T (1976) *Perturbation theory for linear operators*, 2nd edn. Springer, Berlin
- Knox CK, Voth GA (2010) Probing selected morphological models of hydrated Nafion using large-scale molecular dynamics simulations. *J Phys Chem B* 114:3205–3218
- Koldsø H, Shorthouse D, Hélie J, Sansom MSP (2014) Lipid clustering correlates with membrane curvature as revealed by molecular simulations of complex lipid bilayers. *PLoS Comput Biol* 10:e1003911
- Kozlov V, Treshchëv D (1991) *Billiards: a genetic introduction to the dynamics of systems with impacts*. American Mathematical Society, Providence
- Laschewsky A (2003) Polymerized micelles with compartments. *Curr Opin Colloid Interface Sci* 8:274–281
- Leventis PA, Grinstein S (2010) The distribution and function of phosphatidylserine in cellular membranes. *Ann Rev Biophys* 39:407–427
- Li Z, Kesselman E, Talmon Y, Hillmyer M, Lodge T (2004) Multicompartment micelles from ABC miktoarm stars in water. *Science* 306:98–101
- Lowengrub J, Rätz A, Voigt A (2009) Phase-field modeling of the dynamics of multicomponent vesicles: spinodal decomposition, coarsening, budding, and fission. *Phys Rev E Stat Nonlinear Soft Matter Phys* 79. doi:[10.1103/PhysRevE.79.031926](https://doi.org/10.1103/PhysRevE.79.031926)
- Lutz J-F, Laschewsky A (2005) Multicompartment micelles: Has the long-standing dream become a reality? *Macromol Chem Phys* 206:813–817
- Maneta-Peyret L, Lai Y-S, Stefano G, Fouillen L, Brandizzi F, Moreau P (2014) Phospholipid biosynthesis increases in rhd3-defective mutants. *Plant Signal Behav* 9:e29657
- Mouritsen OG (2011) Lipids, curvature, and nano-medicine. *Eur J Lipid Sci Technol* 113:1174–1187
- Peet J, Heeger A, Bazan G (2009) “plastic” solar cells: Self-assembly of bulk heterojunction nanomaterials by spontaneous phase separation. *Acc Chem Res* 42:1700–1708
- Pego RL (1989) Front migration in the nonlinear Cahn–Hilliard equation. *Proc R Soc Lond Ser A* 422:261–278
- Promislow K, Wetton B (2009) PEM fuel cells: a mathematical overview. *SIAM J Appl Math* 70:369–409
- Promislow K, Wu Q (2015) Existence of pearled patterns in the planar functionalized Cahn–Hilliard equation. *J Differ Equ* 259:3298–3343
- Promislow K, Yang L (2014) Existence of compressible bilayers in the functionalized Cahn–Hilliard equation. *SIAM J Appl Dyn Syst* 13:629–657
- Promislow K, Zhang H (2013) Critical points of functionalized Lagrangians. *Discrete Contin Dyn Syst* 33:1–16
- Rapoport A, Rom-Kedar V, Turaev D (2007) Approximating multi-dimensional Hamiltonian flows by billiards. *Commun Math Phys* 272:567–600



- Reed M, Simon B (1978) *Methods of modern mathematical physics. IV. Analysis of operators*. Academic Press [Harcourt Brace Jovanovich Publishers], New York
- Reid W (1988) *Sturmian theory of ordinary differential equations*. Mc-Graw Hill Company, New York
- Rubatat L, Gebel G, Diat O (2004) Fibrillar structure of Nafion: Matching Fourier and real space studies of corresponding films and solutions. *Macromolecules* 37:7772–7783
- Ryham RJ, Cohen FS, Eisenberg R (2012) A dynamic model of open vesicles in fluids. *Commun Math Sci* 10:1273–1285
- Simons K, Vaz WL (2004) Model systems, lipid rafts, and cell membranes. *Ann Rev Biophys Biomol Struct* 33:269–295
- Teubner M, Strey R (1987) Origin of the scattering peak in microemulsions. *J Chem Phys* 87:3195–3200
- Turaev D, Rom-Kedar V (1998) Elliptic islands appearing in near-ergodic flows. *Nonlinearity* 11:575
- van Meer G, Voelker D, Feigenson G (2008) Membrane lipids: where they are and how they behave. *Nat Rev Mol Cell Biol* 9:112–124
- Wang X, Du Q (2008) Modeling and simulations of multi-component lipid membranes and open membranes via diffuse interface approaches. *J Math Biol* 56:347–371
- Zhu J, Hayward R (2008) Wormlike micelles with microphase-separated cores from blends of amphiphilic AB and hydrophobic BC diblock copolymers. *Macromolecules* 41:7794–7797
- Zhu J, Hayward RC (2008) Spontaneous generation of amphiphilic block copolymer micelles with multiple morphologies through interfacial instabilities. *J Am Chem Soc* 130:7496–7502